Soil Inorganic Carbon, the Other and Equally Important Soil Carbon Pool:

Distribution, Controlling Factors, and the Impact of Climate Change

Amin Sharififar[a], Budiman Minasny[b*], Dominique Arrouays[c], Line Boulonne[c], Tiphaine Chevallier[d], Piet van Deventer[e], Damien Field[b], Cécile Gomez[f,g], Ho-Jun Jang[b], Sang-Ho Jeon[h], Jaco Koch[e], Brendan Malone[i], Ben Marchant[j], Manuel P. Martin[c], Alex. McBratney[b], Curtis Monger[k], José-Luis Munera-Echeverri[c], José Padarian[b], Marco Pfeiffer[l], Anne C. Richer-de-Forges[c], Nicolas P.A. Saby[c], Kanika Singh[b], Xiao-Dong Song[m], Kazem Zamanian[n], Gan-Lin Zhang[m,o,p], George van Zijl[e]

[a] School of Agricultural Engineering and Technology, University of Tehran, Karaj, Iran
[b] School of Life and Environmental Sciences, the University of Sydney, NSW, Australia
[c] INRAE, InfoSol, F-45075, Orléans, France
[d] UMR Eco&Sols, Université de Montpellier, CIRAD, INRA, IRD, Montpellier SupAgro, 34060 Montpellier, France
[e] Unit for Environmental Sciences and Management, North-West University, Potchefstroom 2520, South Africa
[f] LISAH, Univ. Montpellier, IRD, INRAE, Institut Agro, Montpellier, France
[g] Indo-French Cell for Water Sciences, IRD, Indian Institute of Science, Bangalore, India
[h] National Institute of Agricultural Sciences, Wanju-gun 55365, Republic of Korea.
[i] CSIRO Agriculture and Food, Clunies Ross Street, Black Mountain, ACT 2601, Australia
[j] British Geological Survey, Keyworth, NG12 5GG, UK
[k] Plant and Environmental Sciences, New Mexico State University, USA
[l] Departamento de Ingeniería y Suelos, Facultad de Ciencias Agronómicas, Universidad de Chile, Chile.
[m] State Key Laboratory of Soil and Sustainable Agriculture, Institute of Soil Science, Chinese Academy of Sciences, Nanjing 210008, China
[n] Institute of Soil Science, Leibniz University of Hannover, Herrenhäuser Straße 2, 30419 Hannover, Germany
[o] College of Advanced Agricultural Sciences, University of Chinese Academy of Sciences, Beijing 100049, China
[p] Key Laboratory of Watershed Geographic Sciences, Institute of Geography and Limnology, Chinese Academy of Sciences, Nanjing 210008, China

*Correspondence: budiman.minasny@sydney.edu.au

Abstract

Soil inorganic carbon (SIC) contributes to up to half of the terrestrial C stock and is especially significant in arid and semi-arid environments, yet has not been explored as much as soil organic carbon (SOC). SIC plays an important role in agriculture, CO_2 sequestration and emission and climate regulation. To address this, a comprehensive review is presented on the digital mapping of soil inorganic carbon including a discussion of SIC vertical variation, its controlling factors, and sequestration/emission capability. We surveyed SIC distribution and mapping efforts in Australia, South Africa, Chile, the Mediterranean basin, Iran, China, France, and the USA. We found that current detailed spatial information on SIC distribution and stock is relatively scarce and digital soil mapping (DSM) efforts to address this are modest. Furthermore, we do not have a complete soil C model that explicitly accounts for all sources and sinks of soil carbon. This review showed that many aspects of SIC in DSM and soil C studies have been so far ignored and that SIC has a crucial role in climate regulation. This review provides some insights into the importance and unknown aspects of SIC.

Contents

Introduction

Soil carbon is recognised as central to soil functioning, plays a crucial role in maintaining the sustainability of soil to produce food, and acts as a large sink of carbon that can mitigate climate change. Soil organic carbon sequestration is a proven, economically viable natural climate change mitigation strategy with multiple co-benefits. However, far less attention has been placed on soil inorganic carbon. The top meter of world soils holds around 2,200 Pg soil carbon, the largest terrestrial store of carbon, of which approximately 1,500 Pg is soil organic carbon. Its counterpart, soil inorganic carbon, has been estimated at somewhere from 700 to more than 1000 Pg (Batjes, 2014; Eswaran et al., 1995). The amount of SIC and SOC stocks down to 2 m of soils is comparable (Zamanian et al., 2021) and SIC has a relatively long mean residence time under natural conditions making it highly relevant in the discussion of soil and climate change (Kuzyakov et al., 2019; Zamanian and Kuzyakov, 2019).

About 30 to 40% of the world's soils are in arid, semi-arid, and hyper-arid areas (Gaur and Squires, 2018; White and Nackoney, 2003). In these areas, SIC can be as important as organic carbon as a carbon store contributing to the CO_2 emissions, as well as, influencing soil physical and chemical properties (e.g. aggregate stability and porosity, water infiltration, pH buffering capacity, and electrical conductivity). SIC comprises up to 90% of soil C pool in these arid areas and in some cases, can contribute up to about 20% and 60% of the whole CO_2 emission from topsoil and subsoil, respectively (e.g. Cardinael et al., 2020). While the rate of CO_2 forming SIC needs further research, notable inorganic carbon sequestration has also been reported (Bughio et al., 2017; Fa et al., 2016; Monger et al., 2015; Okyay and Rodrigues, 2015).

Under natural conditions, it is expected that the SIC mean residence time (MRT) is millennial. However, increased anthropogenic influences could alter the MRT of SIC to annual and decadal time scales (Kim et al., 2020). Recent studies have reported a remarkable contribution of SIC efflux to atmospheric CO_2 due to human activities, including agricultural practices and fertilization (Ramnarine et al., 2012; Zamanian et

al., 2018; Zamanian and Kuzyakov, 2019; Kim et al., 2020). Despite its importance, research on SIC is much less than SOC. A search of the Web of Science bibliometric database shows that from 288,632 papers published with the topic "soil" from 2017 to March 2022, 19% of the papers (53,866 papers) focused on carbon. Of those papers on soil carbon, only 8% considered inorganic carbon or carbonate.

The spatial (vertical and horizontal) variations of SIC at local to global scales are also poorly studied. For example, Lamichhane et al. (2019) reviewed 120 papers on digital mapping of soil carbon and reported that only a few studies have considered SIC and only one study was specifically related to SIC mapping. This lack of attention to SIC is further complicated by the dominance of available models for spatially quantifying SOC that are inappropriate for SIC. Both temporal and spatial variations of SIC can be quite different from SOC, due to horizontally and vertically skewed geographical distribution of SIC because of its pedogenic and geologic origins.

While SOC has featured prominently in global climate change discussions, SIC has not generally been recognised as an indicator or mitigator of change. Most countries do not have detailed maps of SIC and lack assessments showing if land management systems are operating sustainably in relation to SIC and how they will respond to climate change. Agricultural practices such as irrigation can dissolve and remobilise SIC, while application of fertilizers along with lime can change the soil pH and affect the equilibrium between precipitated and dissolved Ca^{2+} and Mg^{2+} and their interactions with CO_2 in soil solution via HCO_3^-. Therefore, accurately modelling the fate and balance of SOC and SIC will allow us to predict how future soil and environmental change will affect the spatial distribution of soil carbon and the functioning of soils. Given the economic and environmental significance of soil and the reliance on soil carbon functions, comprehensive and detailed soil carbon maps (both organic and inorganic) are urgently needed.

Thus, this review aims to:

(1) Outline the contribution of SIC in the global C cycle.

(2) Provide a survey of SIC distribution and mapping efforts around the world.

(3) Provide a comprehensive review of digital mapping and modelling of SIC to identify the current state of the art, research trends and knowledge gaps.

(4) Discuss factors influencing spatial and vertical distribution of SIC, clarify SIC and SOC relationships, and discuss the effects of climate change on the SIC pool.

(5) Identify research needs for furthering our understanding of SIC.

Soil Inorganic Carbon forms

Understanding the natural and anthropogenic processes driving SIC dissolution or re-precipitation is important for calculating soil C budgets, predicting spatiotemporal changes in the total soil C pool, and modelling future scenarios of the global C cycle. Generally, SIC is classified into three groups, based on its origin and formation processes.

<u>Geogenic or lithogenic carbonates:</u> carbonates inherited from calcareous parent materials such as limestone and marls. Geogenic carbonates exist as detrital fragments physically derived calcareous parent materials in place (*in situ*) or as detrital particles transported from other locations (*ex situ*) such as calcareous dust or landslides.

<u>Biogenic carbonates:</u> carbonates formed within terrestrial animals and plants as part of their skeleton, for example, shells, calcified seeds, root hairs, fungal hyphae, bacteria, or released from or within certain organs such as the oesophageal glands of earthworms.

<u>Pedogenic carbonates:</u> carbonates formed authigenically (formed in place from weathering processes) in soils. Pedogenic carbonates form via two pathways: (1) the dissolution and re-precipitation of the SIC pool (i.e. geogenic, biogenic or previously formed pedogenic carbonates, such as nodules) and (2) by the precipitation of Ca^{2+} from silicate weathering and bicarbonate (HCO_3^-) from root and microbial respiration in alkaline soils (Figure 2). Pedogenic carbonate exists in multiple forms and morphogenetic stages that include filaments, coatings, nodules, root casts, pendants, masses, concretions, calcic horizons, and petrocalcic horizons containing laminae, ooliths, pisoliths, and breccia (Ditzler et al., 2017; Gile et al., 1966). These are called caliche, travertine, kankar, or calcrete (Wilford et al., 2015). The carbon contained in all these types is collectively referred to as "soil inorganic carbon". Figure 1 shows a diagram of SIC groups from a broad viewpoint.
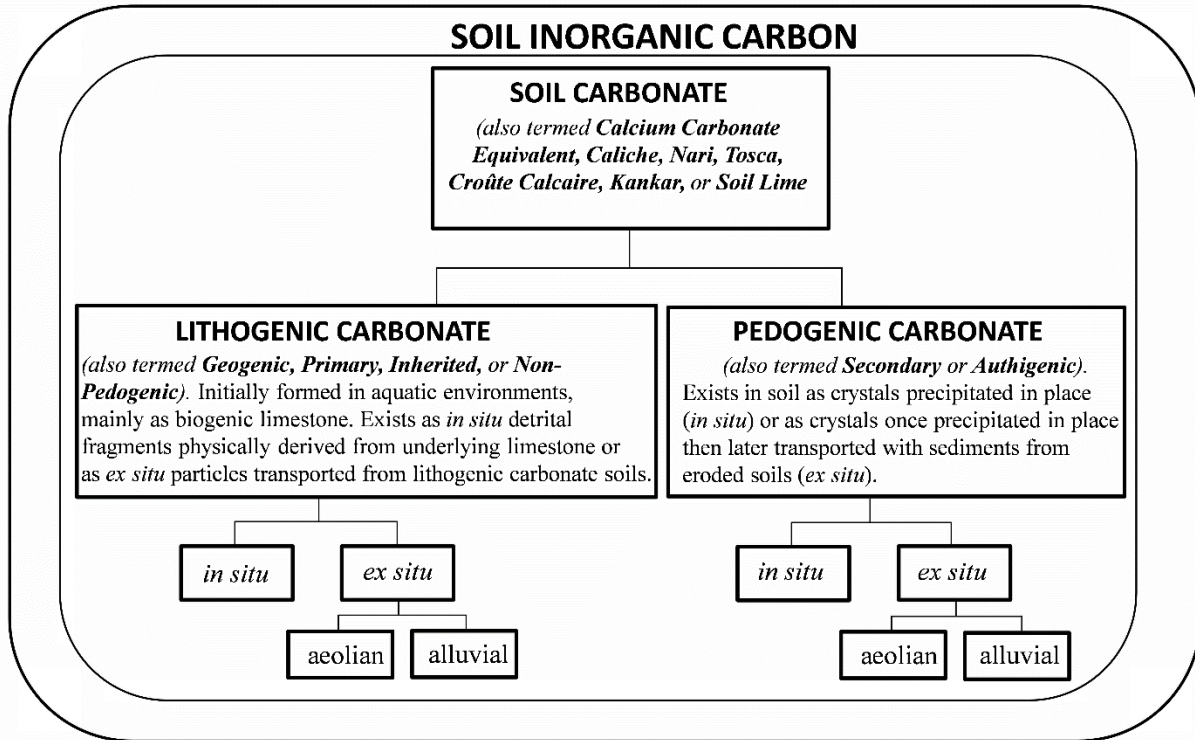
Figure 1. Broad SIC grouping. Each type enters the soil by various *in situ* and *ex situ* pathways. Biogenic carbonate can occur as both lithogenic (e.g., marine shell fragments) and pedogenic (e.g., calcified fungal hyphae) categories. The carbon itself that resides in all types shown above is collectively referred to as soil inorganic carbon. Routine lab analysis involving acid dissolution does not distinguish and separate the various carbonate types. Figure modified from Monger et al. (2015).

The pedogenesis of SIC and the concept of "carbonate generations" can help understand the processes affecting its role as a source and/or sink of CO_2 (Monger et al., 2015). The forms and formation processes of carbonates with specific emphasis on pedogenic carbonates are discussed in Zamanian et al. (2016).

Pedogenic carbonate is derived from the precipitation of carbonate ions derived from the root and microbial respiration reacting with calcium and magnesium from the soil. In one case, the following reactions show the general equilibrium processes:

$$H_2O + CO_2 \leftrightarrow H_2CO_3 \leftrightarrow HCO_3^- + H^+ \qquad (1)$$

$$CaCO_3 + H_2O + CO_2 \leftrightarrow 2HCO_3^- + Ca^{2+} \qquad (2)$$

The reactions are controlled by carbon dioxide (CO_2), pH, Ca^{2+} content and water content. An increase in soil CO_2 or a decrease in soil pH would lead to the dissolution of carbonate, whereas an alkaline

environment would favour the formation of carbonate ions. In addition, the availability of soluble Ca^{2+}/Mg^{2+} is required for the precipitation of Ca/Mg carbonates. If the cations are from the dissolution of pre-existing carbonates, then reactions (1) and (2) apply. If the cations are from the chemical weathering of silicates, then the unidirectional reactions (3) and (4) apply:

$$2CO_2 + 3H_2O + CaSiO_3 \rightarrow Ca^{2+} + 2HCO_3^- + H_4SiO_4 \qquad (3)$$

$$Ca^{2+} + 2HCO_3^- \rightarrow CaCO_3 + CO_2 + H_2O \qquad (4)$$
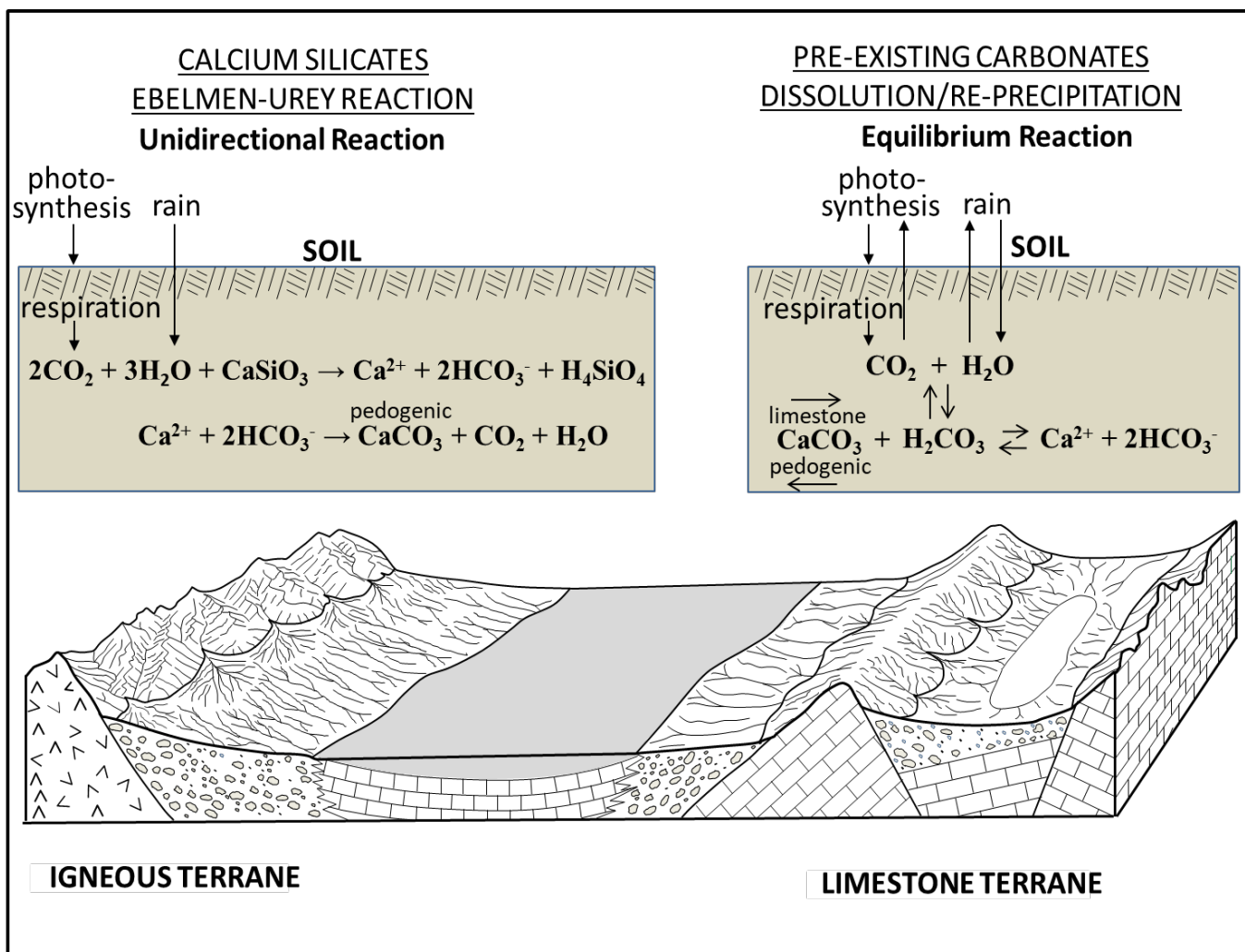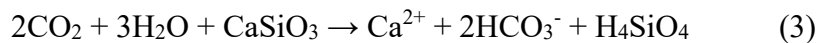
Figure 2. Comparison of the two major pathways of pedogenic carbonate formation. The unidirectional Ebelmen-Urey Reaction involving the weathering of silicates versus the equilibrium reaction involving the dissolution and re-precipitation of existing carbonates (From Monger et al. 2015).

SIC controlling factors

SIC acts as a terrestrial C store and influences soil properties, and thus, we need to understand its spatial and temporal controlling factors before we can work out its spatial distribution. Figure 3 presents a summary of the current understanding of SIC controlling factors as a function of spatial scale. Pedogenic carbonates mainly accumulate in semiarid or arid soils where evapotranspiration is greater than precipitation. Thus climatic factors of mean annual temperature (MAT), mean annual precipitation (MAP), and mean annual evapotranspiration are important indicators on both regional and global scales (Raheb et al., 2017; Zamanian et al., 2016).

As a climate-driven interpretation and distinction of carbonatic soils, classical concepts pedocal and pedalfer soil zones were developed in the USA (Marbut, 1935). Pedalfers refer to soils in the humid regions enriched with Fe and Al sesquioxides; and pedocals refer to soils where evapotranspiration is higher than precipitation with accumulation of carbonates. The continental USA was divided into west dry zone and eastern humid zone based on the pedocal–pedalfer soil boundary called the Marbut line, where mean annual precipitation and evapotranspiration were equal. The Marbut line has been revised using better climatic data and defined in terms of annual water balance equal to zero (D'Avello et al., 2019; Salley et al., 2016). D'Avello et al. (2019) found that the annual water balance was positively related to the depth of maximum $CaCO_3$ accumulation and negatively related to SOC stock. However, this moisture relationship was weak as other factors also control SIC and SOC distribution, such as loess deposition and palæoclimatic environments.

Low rainfall, high temperature and evaporation lead to the retention of atmospherically sourced calcium. However, climate is not the sole controller of carbonate distribution. Proximity to the coast and parent materials are also important factors controlling the distribution of SIC. The type of soil minerals can determine the source of Ca, which can influence SIC formation. Additionally, vegetation could be an indicator of SIC, as soil CO_2 is associated with the respiration of plant roots, decaying organic matter and microbial activity. Microorganisms could also have a role in SIC accumulation by acting as catalysts for soil carbonate dissolution.

SIC controlling factors vary at different spatial extents, although some overlapping might occur (Figure 3). For example, at micro to meso scales, Ca^{2+} availability, pH (in rhizosphere or bulk soil), clay and water content are crucial. At the soil profile to field scale, pH, soil depth, precipitation, leaching, respiration, microbial activity, soil type, nutrients, acid rain, salinity, land use, and fertilization are potential factors

controlling SIC (Ferdush and Paul, 2021). At the landscape scale; topography, land cover, precipitation and temperature are important factors (Guo et al., 2006b). For example, land cover (forest, rangeland, cropland, etc.) with regard to soil management (irrigation, fertilization and tillage) and inherent soil pH can influence carbonate dissolution/precipitation. Topography contributes to deposition and leaching of surface carbonates. At the macro scale (regional to continental scales) climate, land use and lithology are the main drivers of variations in SIC stocks (Figure 3).

Irrigation as an anthropogenic factor can be an influential factor on SIC. It improves biomass production and enhances biological activity i.e. via root and microorganism respiration and increasing CO_2 partial pressure. In turn, it may either lead to enhanced trapping of CO_2 in carbonate-free soils through precipitation of pedogenic carbonates following increased silicate weathering and release of Ca^{2+} ions or decreasing soil pH in carbonate-containing soils, which increases the dissolution of carbonates and CO_2 emission (Gocke et al., 2011). Nitrogen fertilization and liming can affect SIC stocks dynamics, which are discussed in the following sections.

A somewhat ignored factor in assessing SIC spatiotemporal variation is SOC content (Guo et al., 2016; Wang et al., 2015; Guo et al., 2021; Yang et al., 2021; Zhang et al., 2010). SIC and SOC can have positive and negative correlations in different climates and geographic regions. SIC-SOC relationship is discussed in detail, further in this review.
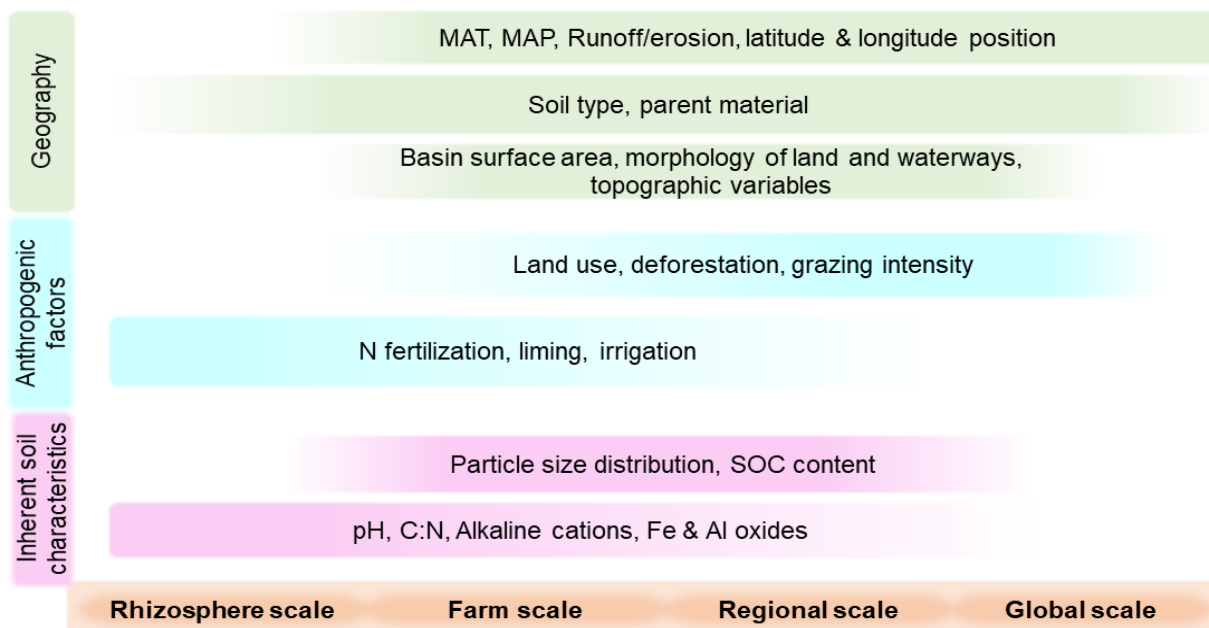
Figure 3. Summary of SIC controlling factors in spatial scales as to inherent soil characteristics, anthropogenic factors and geographical variables.

Vertical distribution of soil inorganic carbon

Unlike SOC which accumulates in the topsoil, the precipitation of SIC occurs mainly in the deeper soil profile. Different trends of depth variation for SIC have been reported in the literature. Land use, soil type, precipitation regimes and erosion/deposition (soil redistribution) all affect the vertical distribution of SIC. The depth distributions of SIC and SOC are usually opposite (Figure 4). An exponential decrease of SOC and a linear increase for SIC with depth has been reported for Belgium with about 13000 soil profiles, where the main controlling factor for SIC variation was geology (Lettens et al., 2004). Batjes (2004) reported an increasing SIC content with depth at regional scales such as arid zones of Kenya as well as in other parts of the world (Batjes, 2014). At the landscape scale, both increase and decrease of SIC content towards the subsoil (≈30-60 cm depth) have been reported (Liu et al., 2014; Wang et al., 2010; You et al., 2020). The changing trend below 60 cm, however, was mostly related to the soil type (Jiménez-Aguirre et al., 2018; Sharififar et al., 2019a). Changes in the amount of SIC in subsoil layers are more conspicuous in arid and semi-arid regions (Raheb et al., 2017; Sharififar et al., 2019a), where low rainfall precipitation leads to carbonate accumulation in the subsoil.
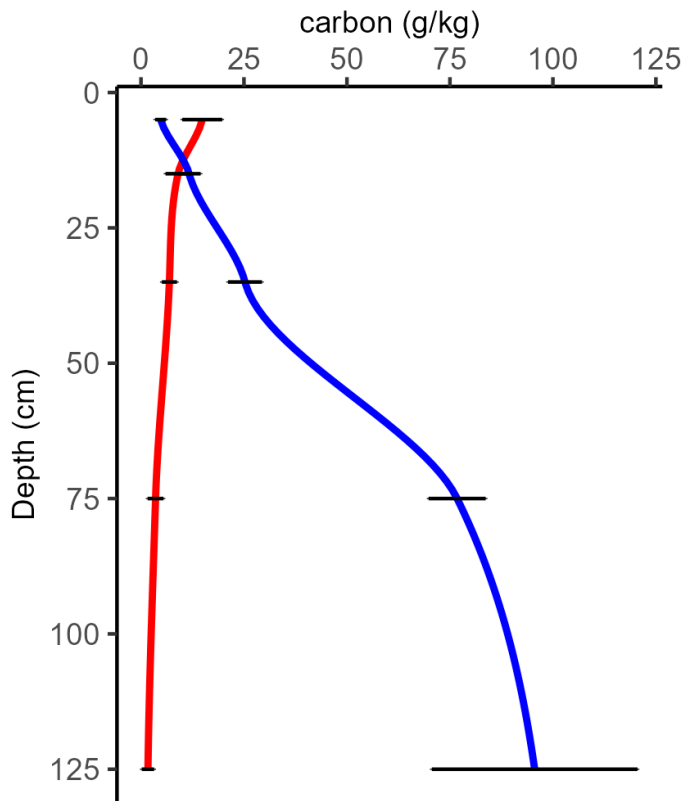
Figure 4. An example of depth variation in a Calcarosol in Australia (Edgeroi area, New South Wales); blue line depicts carbon as $CaCO_3$ and red line depicts carbon contained in SOC (the black horizontal lines show standard errors of measurements at several depth layers).

The depth of pedogenic carbonate in a soil profile is commonly related to rainfall (Retallack, 1994). Jenny and Leonard (1934) found that depth to carbonate (DTC) is a function of mean annual precipitation (MAP), where DTC increases from 350 to 1000 mm of MAP on Mollisols in the central Great Plains of the USA. Retallack (1994) derived a MAP-DTC relationship based on observations of different soil types. This relationship was further improved by Royer (1999) with a larger dataset which found that the depth to the carbonate horizon increased by 360 mm with every 100 mm increase in precipitation (Figure 5).
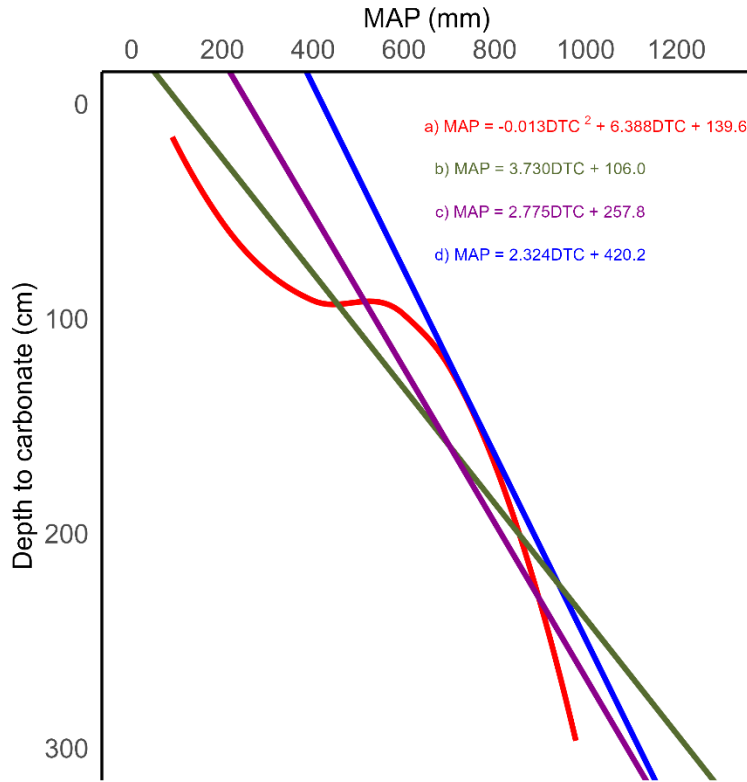
Figure 5. Depth to carbonate (DTC) layer as a function of Mean Annual Precipitation (MAP) using four regression equations from Retallack (1994; equation a), Arkley (1963; equation b), Royer (1999; equation c), Jenny and Leonard (1934; equation d). The graphs are schematic representations of approximate carbonate horizon depth as related to mean annual precipitation. Note that the graphs are redrawn based on findings from the literature from the USA.

Accounting for SIC stock is essential for inventory and calculation of carbon fluxes. SIC storage is calculated for a specific depth layer as follows:

$$SIC_{stock(i)} = SIC_i \times BD_i \times T_i \times (1 - CF_i) \tag{5}$$

where, $SIC_{stock(i)}$ is SIC stock in layer i (kg m^{-2}), SIC_i is the gravimetric SIC content (kg kg^{-1}) in <2mm fraction, BD_i is the bulk density of the whole soil of layer i (kg m^{-3}), T_i is the thickness of the layer (m) and CF_i is the coarse fragment content (>2mm) of the layer (kg kg^{-1}).

If CaCO$_3$ is considered an indicator of SIC, the storage of SIC can be calculated as:

$$SIC_{stock} = (CaCO_3 \times 0.12) \times BD_i \times T_i \times (1 - CF) \tag{6}$$

Where *CaCO₃* is the calcium carbonate equivalent (CCE) concentration (kg kg^{-1}), 0.12 is the conversion factor for CCE to SIC. The SIC stock can be computed for specific areas or biomes by multiplying $SIC_{stock(i)}$ by the area (Rasmussen, 2006).

SIC stock is usually calculated for fractions < 2mm, however inorganic C can exist as coarse fragments, which are usually considered as gravel or rock. Thus, the actual IC stock in the soil profile could be much greater than that being measured. More detailed volumetric sampling and measurement are required to remedy this problem.

Global distribution of SIC and examples from different countries

We need precise and accurate maps of SIC for baseline soil carbon specifications, distribution, modelling, and sequestration/emission assessments for agricultural management and climate mitigation. A global interpretative map of SIC stocks in the top 1 m of soils provided by the United States Department of Agriculture (Eswaran et al., 1993) (Figure 6) shows that SIC amount is comparatively larger in areas with low precipitation. Figure 7 shows the variation in SIC and SOC stocks as a function of geographical latitude. Largely in the northern latitudes and down to 40° south (-40°), an overall inverse relationship can be observed between SIC and SOC stocks. These variations show that SIC stocks are high, where SOC stocks are low and vice versa. This signifies the role of precipitation/evapotranspiration and climate zones on soil C dynamics.

Globally, the distribution of calcareous or carbonate-containing soils is still uncertain with estimates varying from 13% to 40% of the Earth's land surface (Gaur and Squires, 2018; White and Nackoney, 2003; Wilford et al., 2015). This large uncertainty is due to inaccurate mapping representations and differences in definitions. Currently, there is no effort in global data collection of SIC information and no efforts have been undertaken to improve SIC mapping with a fine granular resolution. The map in Figure 6 was created more than three decades ago based on interpretive global soil type maps and climate (Eswaran et al., 1993). There is a lack of knowledge on the current stock, and probable loss or change in SIC. Thus, the following sections provide some details about SIC mapping efforts from different countries with significantly vast areas of soils containing SIC. While this is not an exhaustive list, the survey aims to give a snapshot of the status of SIC mapping in different countries. The case studies were arranged from South to North.
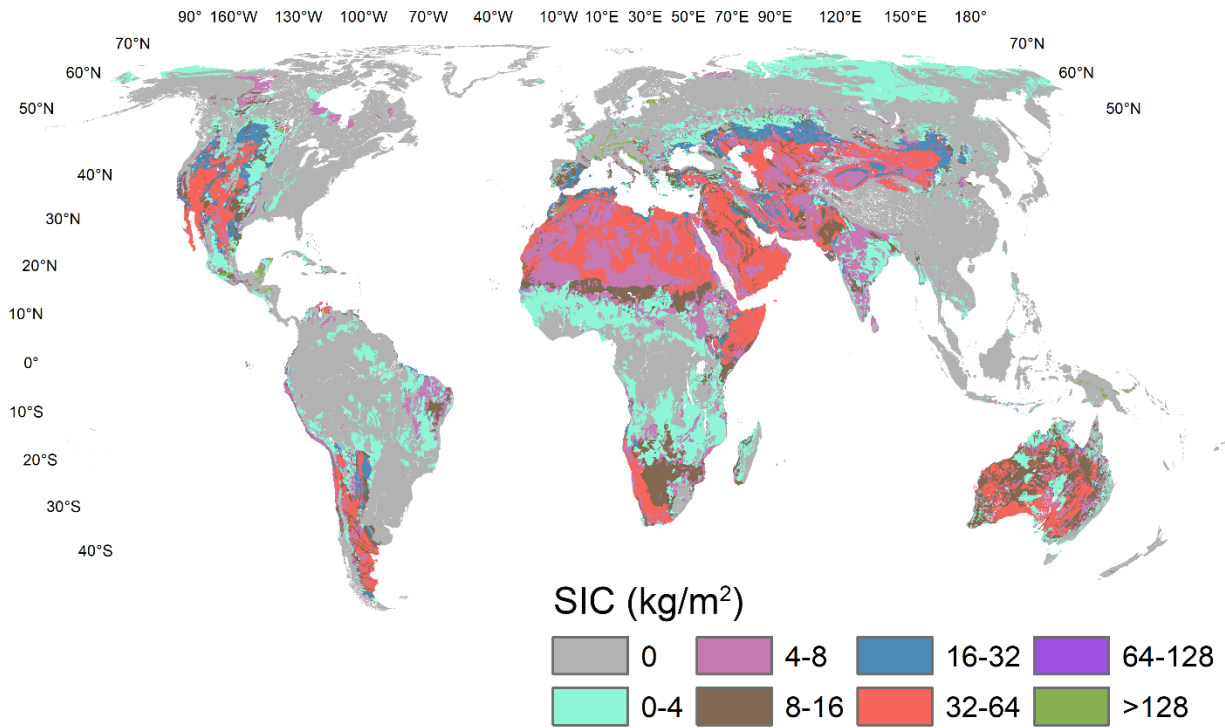
Figure 6. Global variation of SIC to the depth of 1 meter (from United States Department of Agriculture; http://nrcs.usda.gov). Map uses the Equal Earth projection.
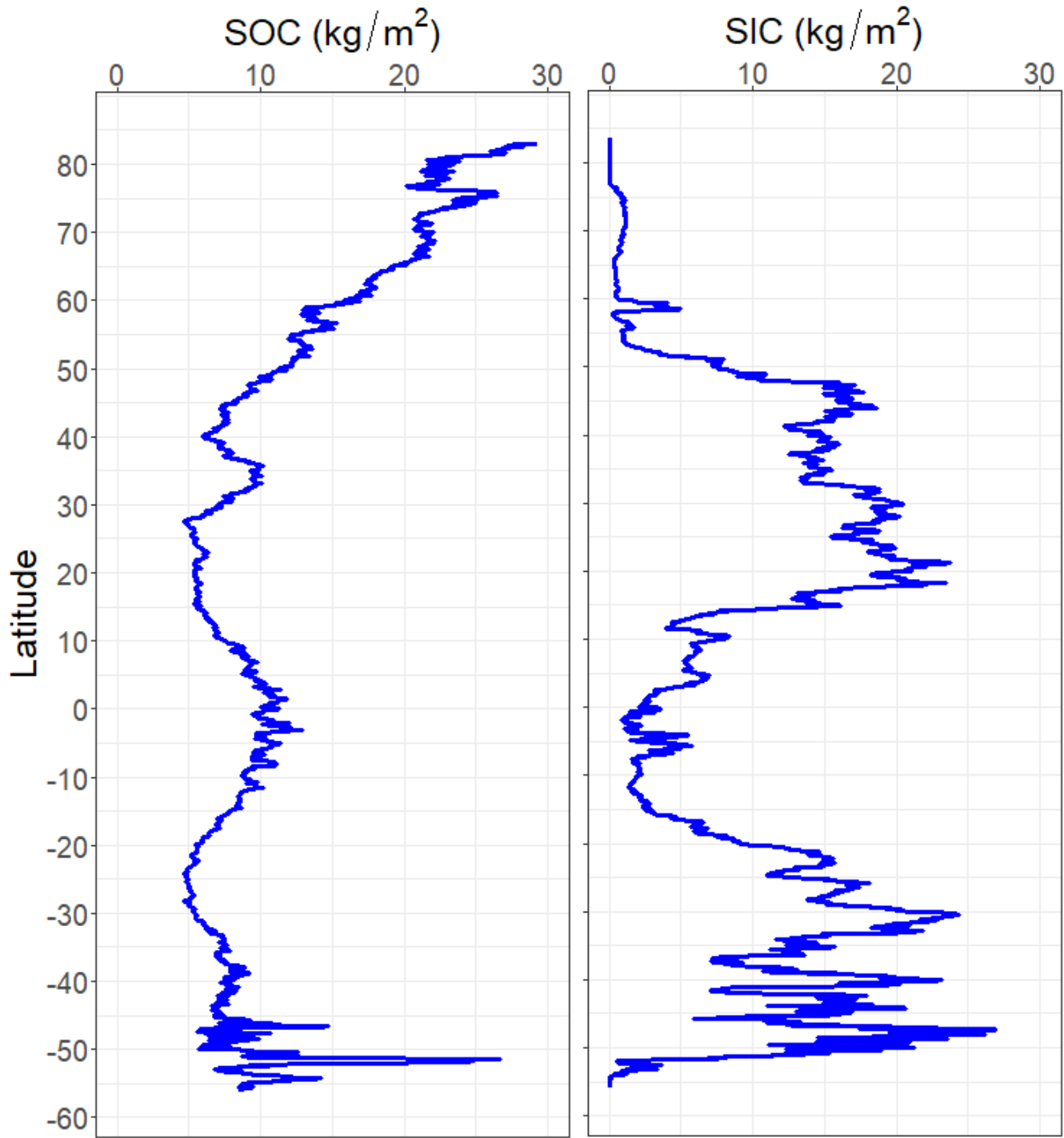
Figure 7. Average SIC and SOC stocks as a function of latitude. Data from global SIC and SOC maps of the United States Department of Agriculture (https://www.nrcs.usda.gov)

In Australia, SIC is predominantly located in arid and semi-arid regions due to low rainfall and biological activity (Ahmad et al., 2015; Wilford et al., 2015). The lack of rainfall results in carbonate relocation in the soil profile rather than being lost due to leaching and is coincident with the lack of biological activity reducing acidity inputs. The retention of Ca^{2+} and Mg^{2+} ions in these areas increases the probability for SIC precipitation and persistence. In addition to *in situ* geological formations, the sources of Ca^{2+} and Mg^{2+} ions include rainfall, sea-spray and aeolian dust. About 90% of the calcium in Australian soil carbonate is attributed to marine sources (Wilford et al., 2015). The persistence of SIC to the south of 30° S is sourced from winter dominated rainfall sourced from rain washed carbonates over the Indian and Southern Oceans, which have significant levels of Ca^{2+} and Mg^{2+} (Wilford et al., 2015). The high rainfall in regions of the eastern margin of Australia, southwest Western Australia, Tasmania and Northern Tropics results in SIC being rare or absent compared to the rest of the continent (Figure 8).

Soils with carbonate have been estimated to cover around 21% to 50% of Australia land surface. A digital soil mapping (DSM) approach in Australia showed different regions of distinct $CaCO_3$ content that resulted in a combination of climate, soil type, parent materials, and vegetation (Wilford et al., 2015). Some distinct areas include aeolian-derived carbonate in western New South Wales (NSW), regolith carbonate in a pocket of the Eastern Highlands in southeast Australia, known as the Monaro Plains, Ca-rich Vertosols in arid and semi-arid regions of NSW and Queensland (QLD). Areas with the largest SIC is in the shallow, highly calcareous soils over the Nullarbor Plain in the south of Western Australia dominated by calcrete, where karstic landforms dominate this region. Other highly calcareous soils are in the Flinders-Mount Lofty ranges and Eyre Peninsula in South Australia.

In the semi-arid region, the soil types also affect the presence and persistence of SOC and SIC. As an example of the profile variations in different soil types, Figure 9 shows the SIC and SOC profile variations in the Edgeroi area in New South Wales, with 9 soil orders according to the Australian soil classification system (Isbell, 2016). Calcarosols (equivalent to Aridisols and Alfisols in the USDA soil taxonomy) show the highest variation and the largest amount of SIC. The changing trend in SIC content in Chromosol (equivalent to Alfisols and some Aridisols), Vertosols (equivalent to Vertisols), Dermosols (equivalent to Alfisols and Ultisols) and Sodosols (equivalent to Alfisols and Aridisols) was increasing down to 60 cm depth and then decreasing down to 100 cm depth. Kurosols (equivalent to Ultisols and Alfisols) and Tenosols (equivalent to Inceptisols, Arisidols, or Entisols) show the lowest accumulation of SIC with no

obvious depth-related changes (Figure 9). The trend of SOC profiles generally shows an inverse relationship with SIC amounts, decreasing down to 20 cm depth.

Climate change scenarios indicate that Australian soil will experience drying by 7% between 2020 and 2050. About 6.5 million km^2 (86% of the land) are estimated to suffer from soil moisture decline of about 10% from 2030 to 2040 as the driest decade (Guglielmo et al., 2021). This will have an impact on SIC distribution.
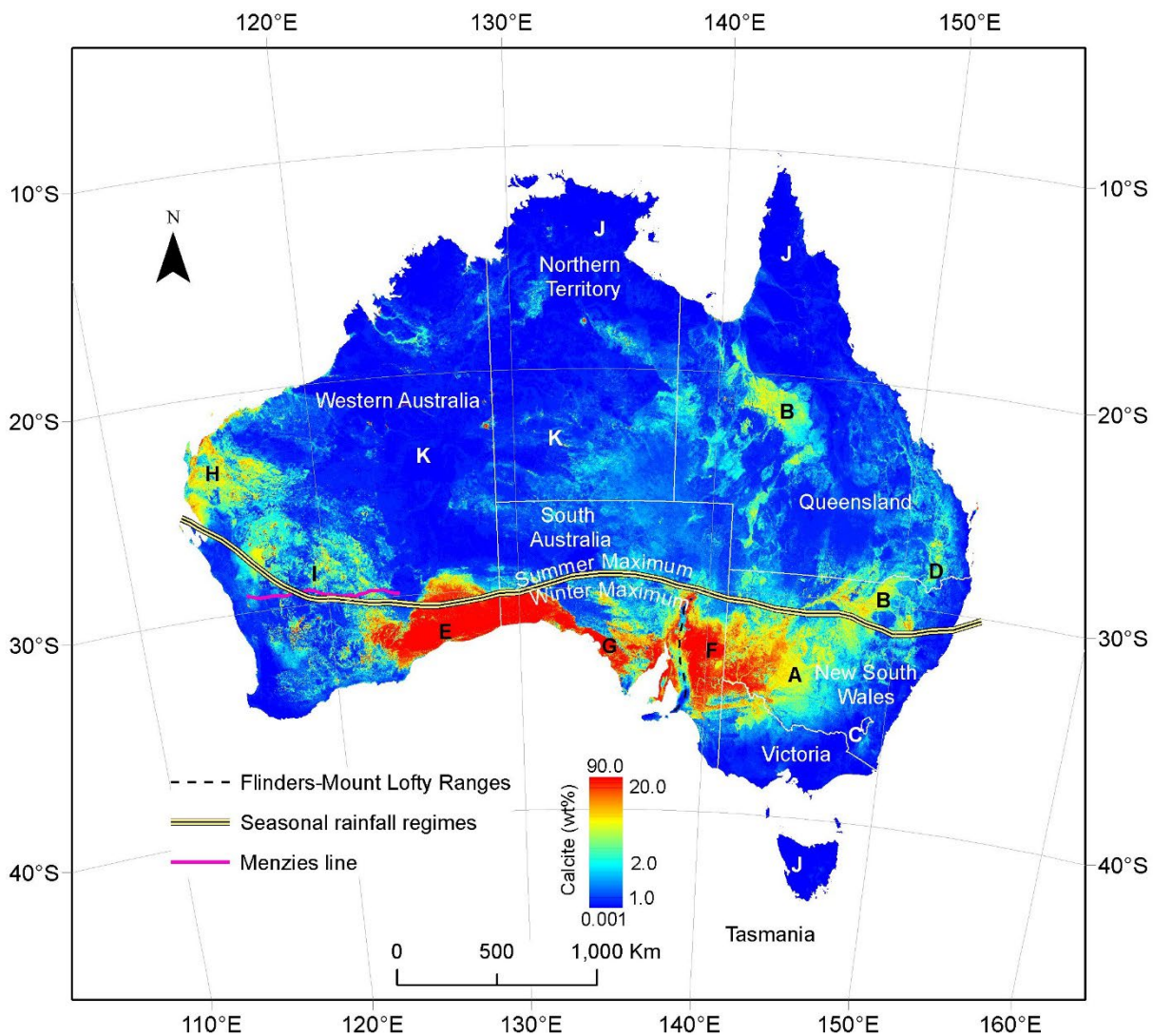

Figure 8. Soil calcium carbonate map of Australia. The yellow line represents the Menzies line delineating a major change in vegetation, and soil and hydrology. Based on Wilford et al. (2015).
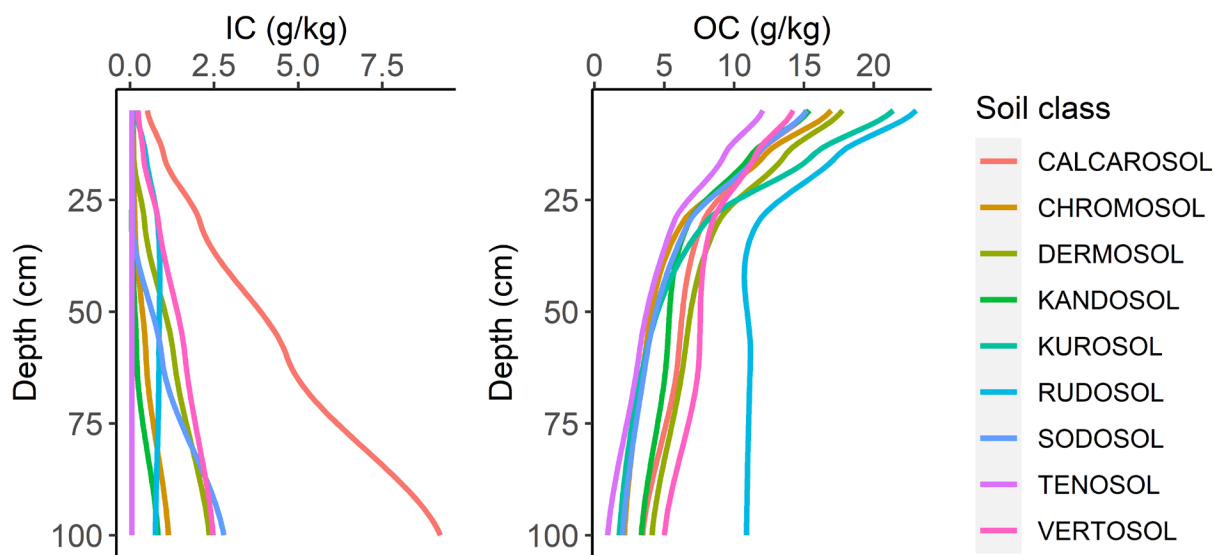
Figure 9. Example of depth variation of soil IC and OC in Australian soils. Each of the displayed soil profile is an average data from several soil profiles.

SIC in Chile

Soil carbonates are common in the dry region of South America, especially in Chile and Argentina. According to the literature, in Chile, soils rich in pedogenic carbonates occur between 18°S and 34°S (Díaz Vial et al., 1960; Pfeiffer et al., 2011), and they reappear in the arid sections of the southern Patagonian Steppe around 52°-53°S (Bockheim and Douglass, 2006; Filipová et al., 2010; Vial, 1965). This distribution is highly correlated with Chile's climatic gradient. The climatic gradient in Chile is extreme and follows a latitudinal gradient from north to south, ranging from the hyperarid environment at the Atacama Desert to the very humid conditions of Patagonian Fjords.

In the Atacama desert, precipitation is less than 20 mm of mean annual precipitation (MAP) below 2000 m above sea level and occurs during sporadic events such as once per decade. Above this altitude, precipitation increases accordingly, rarely exceeding 100 mm/y with rainfall mostly falling during summer, influenced by the south American Monsoon (Garreaud et al., 2009). One of the characteristic features here is the near absence of plants and the presence of highly soluble salts in the soil profiles as a

result of accumulation throughout millions of years of atmospheric deposition (Finstad et al., 2014). These soils contain very low levels of calcium carbonates, as Ca is sequestered into gypsum and anhydrite due to an abundance of SO_4 and the very low levels of CO_2 in soils (Ewing et al., 2008, 2006; Quade et al., 2007). It has been proposed that most of the carbonates are a relict feature from wetter climates with a minimum plant coverage on the surface (Ewing et al., 2006). However, there is evidence of modern occurrences based on δC13 isotopes with low levels of calcium carbonates in which the carbonatic source comes most probably from atmospheric and microbial respiration (Finstad et al., 2016; Pfeiffer et al., 2019). Based on Sr isotope data, the calcium source of carbonates in these soils mostly comes from atmospheric deposition (Rech et al., 2003), as it does not exist in the desert (Owen et al., 2011).

Toward the southern border of the desert, near the modern section of 20-50 mm MAP, there is a transition from gypsic to calcic soils from north to south (drier to wetter). Here, geochemical data indicate that carbonates formed mostly during wetter periods during the Pleistocene (Pfeiffer et al., 2021). Azonal soils in the Atacama Desert influenced by groundwater recharge tend to form carbonate accumulations due to upward flow during evaporation (Hardie & Eugster, 1970; Finstad et al., 2016; Pfeiffer et al., 2018).

South of 26˚S, where the Mediterranean biome is predominant, calcium carbonate soils are a ubiquitous feature in the landscape. This area covered the entire range of precipitations where carbonates are formed according to the literature (Retallack, 1994; Roger, 1999), while between 26˚ S and 33˚S winter rainfall occurs sporadically, creating a blooming desert, which might contribute as the main source of CO_2 since the early Pleistocene (Ebeling et al., 2016). South of 33˚S is an area of marked seasonal precipitation typical of Mediterranean climates with dry summers and wet winters, here carbonatic soils develop on a vast array of parent materials and geomorphic positions, such as andesitic and granitic Hillslopes (Vera, 1985) , marine terraces on calcareous rocks (Pfeiffer et al., 2012, 2011), alluvial deposits (Aburto et al., 2008), andesitic hillslopes (CIREN, 1996a) and palustrine environments (Vargas, 2022; CIREN 1996b). The southernmost soil with the presence of calcium carbonate corresponds to a lacustrine origin soil with a MAP of 790 mm (CIREN, 1997). South of this location, precipitation increase systematically toward the south, consequently disappearing the climatic conditions that allow pedogenic carbonates to form. This incompatibility for calcium carbonates to form is increased by the dominance in the landscape of Andisols derived from volcanic ash, which tends to be acidic.

In Chilean Patagonia, a common characteristic is a complete time "reset" after the last glacial maximum (LGM), as the entire region was covered with ice then. The region's extent and intensity of glacial erosion

resulted in the absence of soils older than the LGM. Over this young landscape acts a climatic gradient with precipitation that ranges from 8,000 mm in the western fjords to 200 mm in the eastern pampas allowing very different soils to converge in a few kilometres. A particular feature of carbonatic soils in this region is that they are formed over glacial and fluvioglacial deposits (Bockheim and Douglass, 2006; Douglass and Bockheim, 2006) and many of them present cryogenic properties (Bockheim et al., 2009). While precipitation could be lower enough to form well-developed calcic soils, they show early development stages (Bockheim and Douglass, 2006; Filipová et al., 2010), most probably related to their young age and the low temperatures predominant in the area.

A recent digital soil mapping estimate of carbon stocks for Chile up to 1m depth (Figure 10), estimated SIC by around 1.4 Pg, being only a small fraction of SOC stock of Chile which was around 21.5 Pg (Padarian et al., 2022). Given the observed increasing content of SIC in depth, we expect that the stock would increase considerably at lower depths. This highlights the need for specific surveys with observations beyond the traditional 1 m depth.

Intensive agriculture may accelerate the loss of SIC. For example, Kim et al. (2020) found a decrease of 36% in SIC stock at a Pampas grassland site at 34ºS in Argentina. Future climate change scenarios suggest that there would be a small decrease or no change in rainfall over Chile but a clear warming trend over northern and inland regions (Williams, 2017). It is still unclear how these will affect SIC stock in the region.
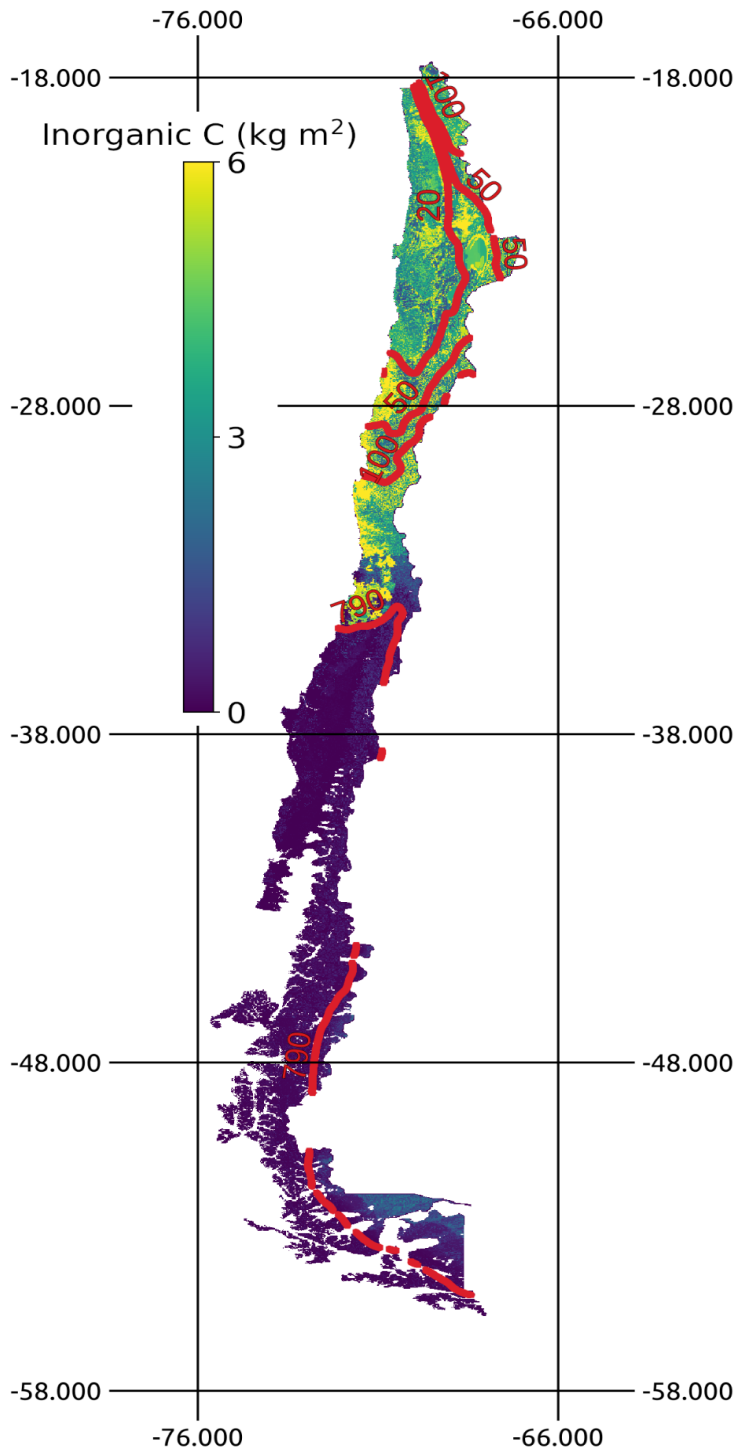
Figure 10. Distribution of SIC stock to 1 m depth in Chile.

Calcareous soils in South Africa are quite widespread. In the local classification system, calcareous soils are placed in 31 out of the 145 recognized soil types (Soil Classification Working Group, 2018). The climatic border of the calcareous soils is regarded as the area with a Weinert N-value greater than 5 (Figure 11; Weinert, 1980). The Weinert N-value is calculated as in Equation 7:

$$N = 12 \times Ej/ MAP \qquad (7)$$

Where N is the Weinert N-value, Ej is the evaporation in January, the hottest month in South Africa, and MAP is the mean annual precipitation.
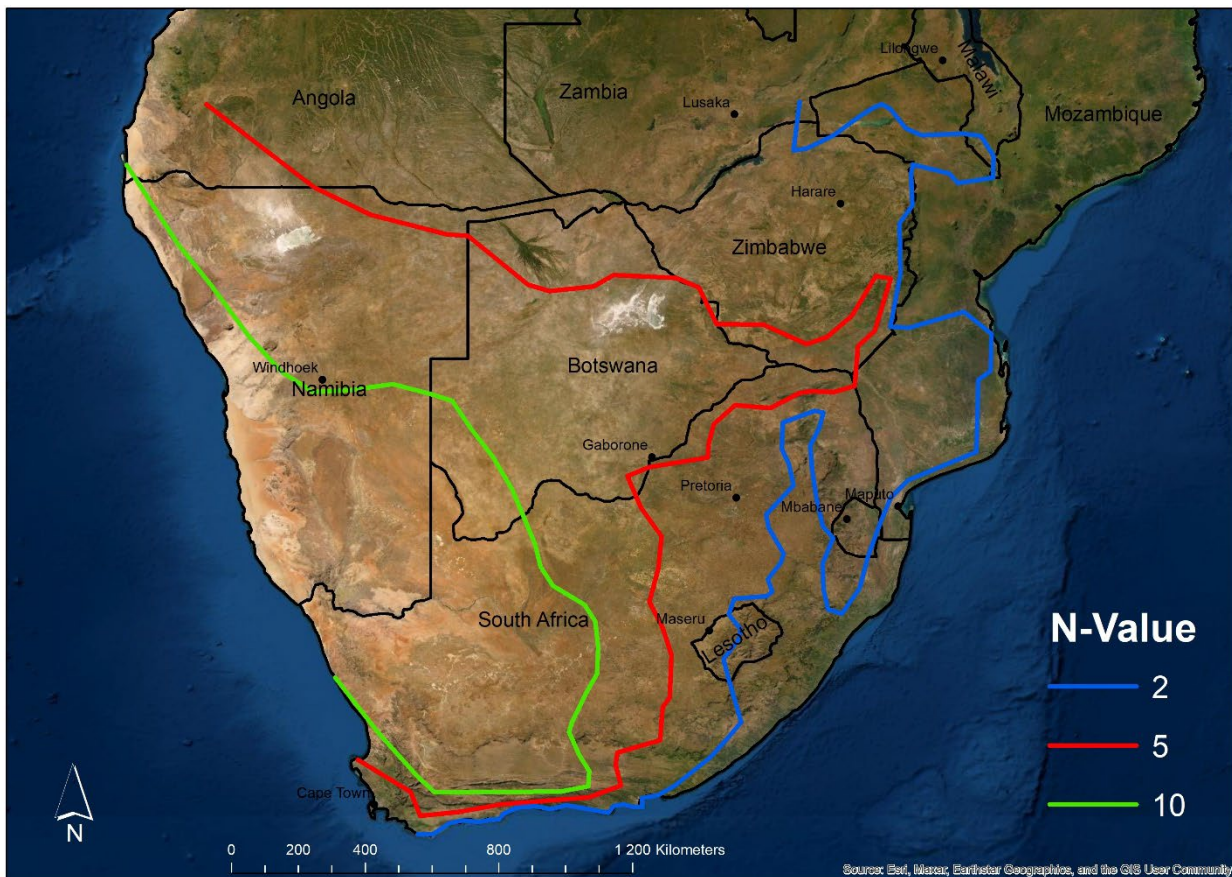
Figure 11. Weinert N-values for southern Africa (based on Jordaan et al., 2017).

An interesting phenomenon that leads to calcareous soils is the occurrence of giant earth mounds locally called heuweltjies (Afrikaans for small hills), created by the southern harvester termite *Microhodotermes viatorare* (Picker et al., 2007). These heuweltjies occupy 14-25% of the land in the southwestern parts of

south Africa (Lovegrove and Siegfried, 1986). The soils within these heuweltjies are often calcareous, due to the Ca^{2+} and CO_3^{2-} enrichment by termite activity, as well as the decrease in soil moisture due to the mound structure (Fey, 2010). The increased fertility of the heuweltjies and the drier soil moisture regime give rise to a different vegetation structure, clearly visible on satellite images (Figure 12).

Figure 10. Typical heuweltjie patterns from a Google Earth image near Robertson in the Western Cape of South Africa.

Anecdotal evidence suggests that calcareous soils also occur within the first dune from the sea, all along the South African coast, from the area west coast to the tropical east coast, due to carbonates being wind-blown from the sea (F Ellis, personal communication). The only exception is in the southern and eastern cape, where the process of acidification through podzolization overrides that of calcification.

There have been efforts to map the calcareous soils in South Africa, and a distribution map could be created from the land type survey (Figure 13; Land Type Survey Staff, 1972-2002), which was conducted to determine the agricultural potential of South Africa's soils. The map units are polygons grouping areas

with similar macroclimate, geology and soil distribution patterns at a scale of 1: 250 000 (Paterson et al., 2015). Each polygon has an accompanying inventory showing an approximation of the percentage cover of different soil types on each terrain unit within the land type. Therefore, the final map gives an idea of the distribution of calcareous soils, rather than an accurate depiction of exactly where they occur. No attempt has been made to quantify the carbon stocks, although it could be vast as the soils cover large areas and the thickness of the calcareous layers can vary between a few millimetres up to 200 m thick.
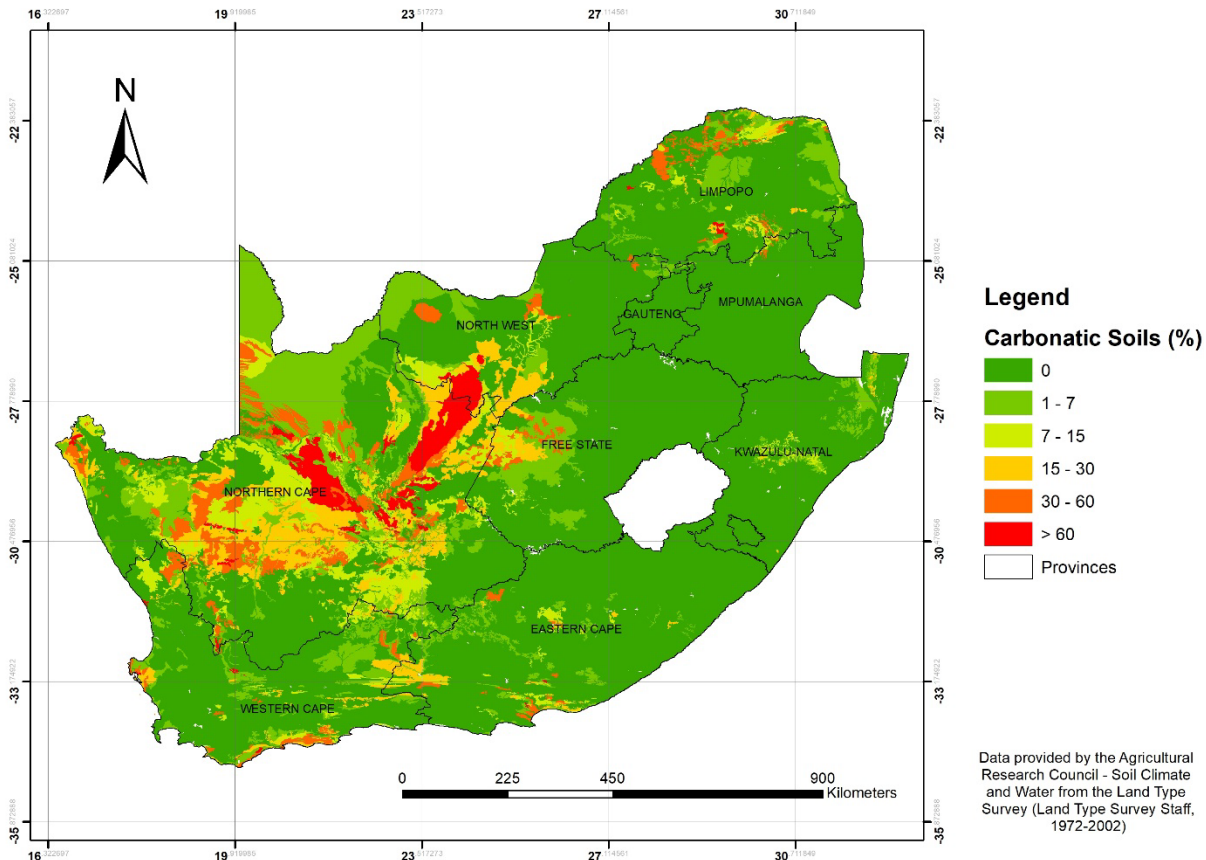
Figure 11. Distribution of the percentage of carbonatic soils in South Africa at a national scale based on interpreting polygons of the land type survey (Land Type Survey Staff, 1972-2002; Le Roux et al., 2013).

SIC in the Mediterranean Basin

In the Mediterranean basin, soils are mostly developed on calcareous rocks. Calcisols, Leptosols, Cambisols and Luvisols (FAO, 2014) are dominant soil types (Jones et al., 2005) and often contain various morphologies and concentrations of carbonates. Areas of Mediterranean conditions cover 5% of the

world's SIC stock. The major types of carbonate minerals are calcite ($CaCO_3$) and dolomite ($MgCO_3$). For example, Díaz-Hernández et al. (2003) measured 81 profiles located in Southeast Spain and reported an average of 134 kg m^{-2} (1340 t SIC ha^{-1}), of which 88 kg m^{-2} was in the form of calcite and 46 kg m^{-2} in the form of dolomite in the 0-2 m depth layer.

In the Near East North Africa (NENA) region, calcareous soils are common and the stocks of SIC are often higher than those of SOC. In the topsoil (0-0.3 m), the SIC stock ranged between 25 and 120 t ha^{-1} compared to 12-35 t ha^{-1} for SOC. In subsoils (0.3-1m), the difference in stocks is even larger, the SIC ranged between 2.5 and 45 kg m^{-2}, compared to 2-4.5 kg m^{-2} for SOC (Darwish et al., 2018). Under Mediterranean conditions, the SIC stocks show high spatial variation in different geographic locations. For example, Lebanon, Gaza, Jordan, Mauritania, Sudan show relatively low SIC stocks with average values lower than 5 kg m^{-2} in topsoil and lower than 10 kg m^{-2} in subsoils, while Egypt has much higher values with average mean stocks exceeding 10 kg m^{-2} in topsoil and 20 kg m^{-2} in the subsoil. Brahim et al. (2012) measured SIC contents in all soil groups of Tunisia with high disparities such as reduced concentration (<1 g SIC kg^{-1} soil, or < 0.1%) in Podzoluvisols, medium concentration in Solonchaks and Gleysols with about 16 g SIC kg^{-1} soil, and high concentration in the other soils with mean SIC concentration up to 24 to 36 g SIC kg^{-1} soil in Luvisols and Lithosols.

Densely populated with a semiarid climate and long history of agriculture, Mediterranean soils face several threats to global changes: soil losses, salinization and SOC depletion (Lagacherie et al., 2018). Particular attention must be paid to the effect of climate changes on the Mediterranean region, where increased temperature, increased frequency of extreme events such as heat waves and decreased and more concentrated rainfall are forecast (IPCC, 2007). Increasing temperature and dry-wet cycles have been largely described to affect SIC dynamics (Lapenis et al., 2008; Tao et al., 2022). A study for Northwest Tunisian calcareous soils indicated a moderate and positive response of soil CO_2 emission to temperature. Q_{10} (the proportional change in respiration with a 10 C° increase in temperature) was measured at 1.7 and ranged around 2.6±1.2, given in the literature (Hamdi et al., 2013). At first sight, these Tunisian calcareous soils seem to have no specific response to temperature increases, but extra CO_2 is emitted from both SOC and SIC pools with increasing temperature (Chevallier et al., 2016). There are not enough studies focusing on how and under what conditions the large SIC pool of the Mediterranean soils may affect climate change and vice versa. A better understanding of SIC dynamics and its role in ongoing global changes is particularly critical for Mediterranean areas, where SIC is the most important C form.

In Iran, various climatic situations have created diverse bioregions and soil types (Roozitalab et al., 2018a). In the country's northern provinces, sub-humid and humid climate overshadows the soils and their properties, resulting in lower carbonate accumulation, while in the south, central and eastern areas with arid and semi-arid climate and geological deposition and lithology, there is a much higher inorganic carbon even in topsoil. About 41% of Iranian soils are Aridisols and 41% Entisols (Roozitalab et al., 2018b), which shows that the soils are mostly young in terms of development and that the depth to carbonate accumulation is not as deep as areas with high rainfall. Due to low rainfall in many parts of the country, carbonates leaching has not happened as much as in the northern regions neighbouring the Caspian Sea.

Case studies and technical reports of local research carried out by the National Soil and Water Research Institute show that carbonates are accumulated at around 30 cm depth in a vast majority of soils and often show various increasing and sometimes decreasing trends below this depth. Geomorphology and parent material play a major role in Iranian soil variation and the distribution of SIC (Eghbal et al., 2018). Calcification, and carbonates redistribution in soil profiles are among the major soil development factors in arid and semi-arid areas of the country, which can be the main drivers of SIC spatiotemporal variation (Khormali and Toomanian, 2018). There is an observable trend of SIC variation in different soil types, even in areas with similar climatic and physiographic situations. Figure 14 shows an example of SIC and SOC depth variations in a typical semi-arid region in Iran with regard to different soil types. As can be seen in Figure 14, SIC and SOC show inverse and diverse variations with depth. This example shows that SOC usually has a decreasing trend with depth, while SIC can increase or decrease with depth, which is normally expected in arid and semi-arid regions of Iran. Deposition and soil redistribution by surface phenomena, which are perceivable from the soil types, are drivers of such diverse variation in SIC with soil depth (Sharififar et al., 2019; Sharififar, 2019). The graphs presented here (Figure 14) are regarded as typical examples for wide areas of Iran under arid and semi-arid climatic situations and calcareous geological structures/parent material.

As in many other parts of the world, no systematic and sufficient studies have been done on SIC spatiotemporal modelling and mapping in Iran and currently, there is no national digital soil map for SIC. This fact implies the need for further SIC mapping and exploration to understand its interactions with climate change, and C cycle at the national scale.
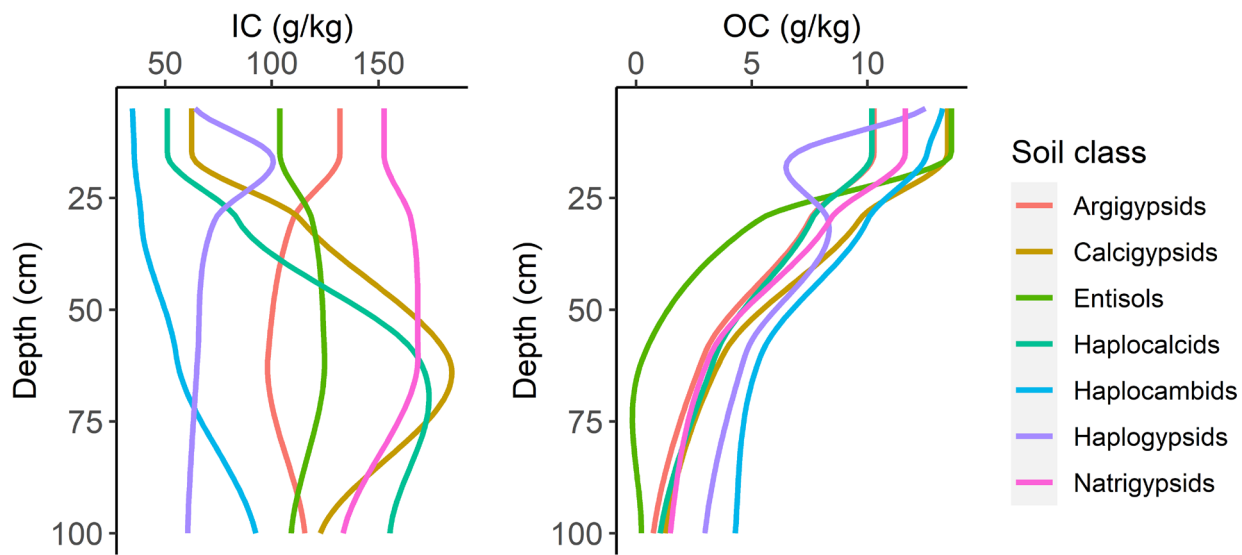
Figure 12. Example of SIC (IC) versus SOC (OC) variations with depth for different soil types in a typical semi-arid region of Iran. Each of the displayed profile is an average data from several soil profiles (adapted from Sharififar, 2019).

SIC in China

Over one-third of China's land is characterised as arid and semiarid biomes (Xia et al., 2017), in which pedogenic inorganic carbonate accumulates. In general, the topsoil SIC contents are positively correlated with aridity and negatively correlated with air temperature (Mi et al., 2008). Therefore, the SIC contents significantly decline from west to east and from north to south of China (Wu et al., 2009). SIC storages in subsoils were much greater than those in topsoils. For the upper 3 m, approximately 42% of the SIC was found in the depth of 2-3 m. The estimated SIC stocks at soil depths of 0-1 m, 0-2 m and 0-3 m were 53.58±0.57 Pg, 134.96±0.91 Pg and 232.21±1.21 Pg, respectively (Song et al., 2022).

Song et al. (2022) conducted spatiotemporal modelling of the SIC pool across China's main ecosystems (i.e., cropland, forest and grassland). Soil samples were collected from 13769 sites across mainland China in the 1980s (n=7299), 2000s (n=774) and 2010s (n=5696). The paired contrasts were selected from samples in the 1980s and 2010s, with a distance of less than 50 km, followed by a paired t-test to evaluate the changes in SIC by taking the soil samples in the 1980s as the baseline. Overall, the study found a significant decrease in SIC stock in the upper 30 cm of soil surface (11.33 g C m^{-2} yr^{-1}) during 1980-2010

(Figure 15a). Over 30 years, the SIC of cropland, forest and grassland declined by 0.34 kg m^{-2} (3.4 t ha^{-1}), 0.38 kg m^{-2} and 0.35 kg m^{-2}, respectively. Nevertheless, high prediction uncertainty (i.e., high standard deviation values) was found in areas with high SIC (Figure 15b). For the topsoil (0-30 cm), the mean values of SIC maps in 1980 and 2010 were 1.64±0.14 kg m^{-2} and 1.50±0.14 kg m^{-2}, respectively. During the last three decades, the total SIC pool declined by 1.37±0.37 Pg (8.99±2.24%) (Figure 15a), most of which may have been released as net CO_2 emission (a maximum of 89.22 Tg yr^{-1}).
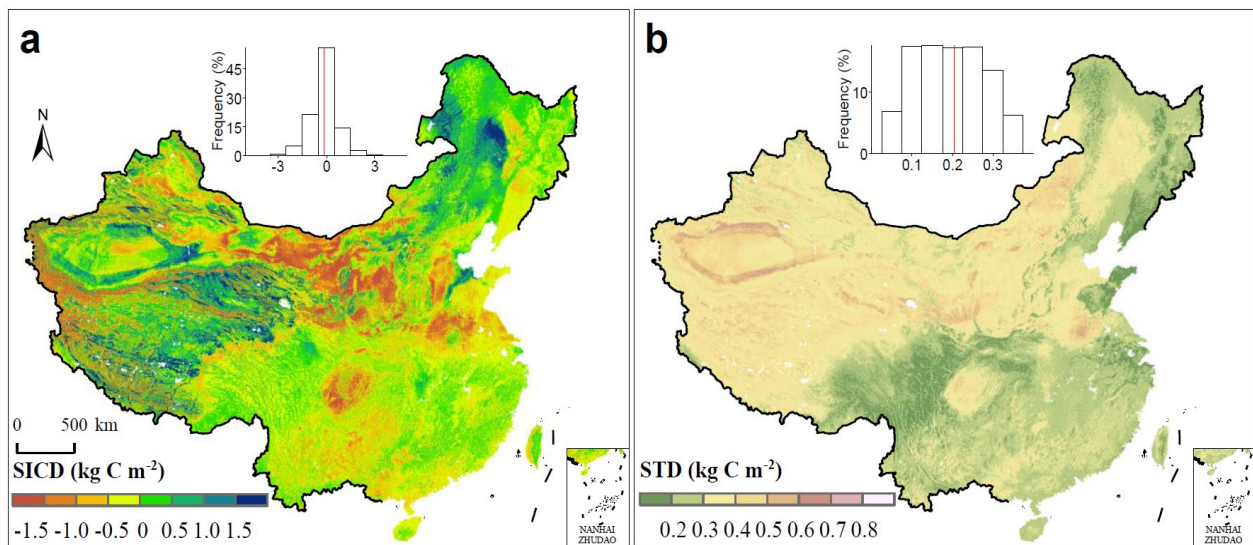
Figure 13. (a) SIC changes in topsoil (0–30 cm) across China from 1980 to 2010 (negative values refer to SIC loss); (b) standard deviations of variations in SIC changes. The red line of the histogram at each map indicates the mean value. Adapted from Song et al. (2022).

China has experienced rapid land use changes and intensified agriculture by wide application of chemical fertilizers over the past several decades. Our study (Song et al., 2022) shows that soil acidification caused by global change, atmospheric nitrogen (N) deposition, and N fertilizers has greatly accelerated SIC loss. Assuming the spatial controls continue, the potential changes in total SIC stock were projected under two Shared Socioeconomic Pathway (SSP) scenarios, including SSP1-2.6 and SSP3-7.0 of Coupled Model Intercomparison Project Phase 6 (CMIP6) models that represented the low and medium/high radiative forcing, respectively. Overall, approximately 19.12-19.47% of the SIC stock in China, equivalent to 2.69-2.74 Pg C, could be further lost by 2100 when taking the 2010s as baseline. Notably, under SSP1-2.6 scenario, SIC in natural ecosystems (forest and grassland) may decrease by 12.82%, while 31.27% of the SIC in cropland might be lost.

The consumption of SIC may offset a large portion of the efforts of SOC sequestration practices, which emphasizes the importance of an updated SIC inventory for global terrestrial carbon pool estimates. The indirect coupling of reactive nitrogen and inorganic carbon through soil reactions, in addition to routine biotic carbon and nitrogen coupling should be considered for a complete picture of global carbon and nitrogen cycling.

SIC in France

Using the French systematic soil quality monitoring grid (RMQS, Arrouays et al. (2002)), design-based estimates of the mean and total amounts of SIC content and stocks and their associated uncertainties have been produced following the approach recommended by Brus and Saby (2016). Design-based estimation of means or totals from systematic random sampling is straightforward: the sample mean is an unbiased estimator of the population mean. These estimates are also precise, thanks to the good spatial coverage of the observations. However, this is not the case for the sampling variance of the estimated mean (or total), i.e. the variance of the estimated mean (or total) over repeated systematic random sampling. Therefore, we approximated this quantity by multiplying the simple random sampling approximation by Geary's spatial autocorrelation index (D'Orazio, 2003). This approach is more straightforward to implement than the one retained by Marchant et al. (2015) which required geostatistical simulations.

Here, we provide estimates for 0-0.3m and 0.3-0.5m and compare them to SOC estimates (Table 3). We also provide the percentage of sites where SIC>SOC and the mean value of SIC content for these sites. Soil inorganic carbon (SIC) was calculated from the calcimetry analysis ($CaCO_3$ equivalent) multiplied by 0.12. The detailed analytical protocol is available in Marchant et al. (2015). Figure 16 shows the distribution of SIC density in France.

Table 3. Summary statistics of soil inorganic and organic carbon in French soils (including Corsica) obtained from RMQS.

Variable	Units	0-30 cm	30-50 cm	0-50 cm
Mean SIC	g kg^{-1}	6.55 (0.29)	7.27 (0.35)	6.48 (0.32)
Mean SIC density	kg m^{-2}	1.89 (0.086)	1.421 (0.071)	3.15 (1.48)

Total SIC stock	Pg	1.025 (0.047)	0.712 (0.037)	1.737 (0.082)
Mean SOC	g kg^{-1}	25.18 (0.32)	10.50 (0.22)	17.51 (0.28)
Mean SOC density	kg m^{-2}	6.74 (0.06)	1.98 (0.04)	8.41 (0.09)
Stock_SOC_France	Pg	3.65 (0.034)	0.99 (0.02)	4.64 (0.053)
Area SIC>SOC	%	10.95	13.36	10.5
Mean SIC>SOC	g kg^{-1}	44.83(0.94)	41.4(1.06)	43.4(1.01)

Values represent means and standard errors in parenthesis. The standard errors were corrected with a factor that is a function of Moran's index of spatial autocorrelation. The number of sites with available data used for calculations was 2161 for 0-30 cm, and 1998 for 30-50 cm.

The total SIC stock values for 0-0.3 m were relatively similar to those obtained by Marchant et al. (2015). They also mapped topsoil SIC in France and evidenced that "the largest values were recorded in the calcareous and shallow chalky soils of the Champagne region, on the Jurassic rocks of the Charente region (southwest France) and on various calcareous rocks of the Mediterranean region of southern France". This suggests that the main controlling factors of SIC stocks in French topsoil are the calcareous content of the parent material, its friability, and the rejuvenation of soils, either by deep ploughing (vineyards) or erosion (calcareous mountains). Note also that frequent ploughing of cropping soils may lead to rock fragmentation and thus to an increase of SIC in fine earth fraction. Indeed, the estimates that we provided are only related to SIC in < 2mm fractions. Therefore, large amounts of SIC contained in coarse elements are ignored by these estimates. The total SIC stock may be slightly underestimated for soils developed on dolomitic parent material, as magnesium carbonate is harder to extract with acid than is calcium carbonate. The mean value of SIC where SIC>SOC does not show very large local variabilities. These estimates are limited to the upper 0.5 m of soils.

Under the French climate, and without the rejuvenation of calcareous soils, the natural evolution of French soils is progressive acidification. This is why liming is applied on a large proportion of cropped soils. Saby et al. (2017) noted a small increase in pH of French non-calcareous agricultural soils using large datasets on analysis requested by farmers between 1996 and 2010. Though it can be considered beneficial

for agronomic and soil structure stability points of view, the amount of lime applied to French soils and their dynamics in topsoil is unlikely to change the global estimates significantly.

Some authors argue that deep weathering of some non-calcareous soils may increase deep soil carbon sequestration when the source of Ca is the weathering of other Ca-bearing minerals (e.g. Cromack Jr et al., 1979; Landeweert et al., 2001). Additionally, amending soils with crushed calcium- and magnesium-rich silicate rocks may lead to an increase of atmospheric CO_2-derived dissolved inorganic carbon that may then be further sequestered in soils through the formation of carbonate minerals (e.g. Beerling et al., 2020). There is, however, little evidence that this is feasible in the French context.

The total SIC stocks in mainland France topsoil (0-0.3m) in fine earth are less than three times the total SOC stocks to the same depth. Given the potential of additional carbon sequestration by SOC recently estimated for mainland France (1.8 per mil, Martin et al. (2021)), they are unlikely to contribute to substantial additional C sequestration, and the main issue should be to act against acidification. However, these SIC stocks are somewhat similar to the SOC stocks for the 0.3-0.5 m layer. This is because SOC stocks sharply decline with depth and some chalky and calcareous soils have very high SIC stocks in this layer. In summary, without deeper analysis, it cannot be stated that France is ready to put in place reliable and efficient actions to increase SIC sequestration in its soils, especially if the overall objective is to mitigate GHG in the atmosphere.
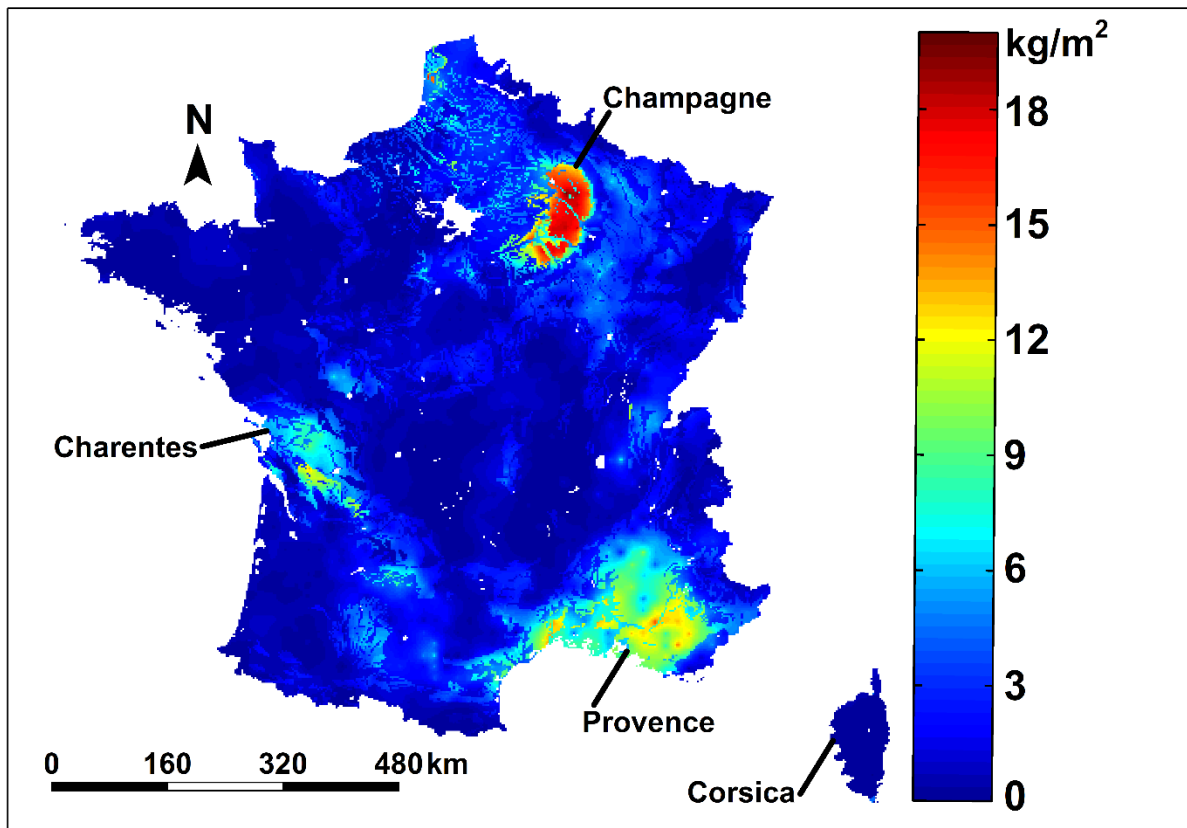
Figure 14. Map of topsoil (0-0.3 m) SIC density in mainland France, including Corsica (based on Marchant et al., 2015).

SIC in the United States of America

The distribution of SIC in the United States is shown in Figure 17A. The map is based on the STATSGO database of the USDA-NRCS (Ditzler et al., 2017). At the broadest scale, the USA is divided into Land Resource Regions (LRRs). These are units based on a synthesis of physiography, geology, climate, water resources, soils, biological resources, and land use (NRCS, 2006). The LRR divisions, which are labelled alphabetically from the Northwest to the Southeast, are shown on both the SIC map and Land Use map (Figure 17A and 17B). An analysis of the amount of SIC in the LRRs was made based on the minimum, midpoint, and maximum amounts of calcium carbonate equivalent recorded in STATSGO (Guo et al., 2006a). The results show that the greatest amount of SIC occurs in the arid and semiarid LRR-D, LRR-H, LRR-I, and LRR-J (Figure 18). The glaciated upper Midwestern regions that contain large amounts of detrital lithogenic carbonate also have high amounts of SIC (i.e., LRR-M and LRR-F). Humid regions,

32

such as LRR-A, -N, -O, -P, -R, -S, and -U have little or no SIC. The total SIC for the conterminous USA ranges from 22.6 to 93.7 Pg with a midpoint amount of 54.1 Pg (Guo et al., 2006a).

Pedogenic carbonate is linked to bioclimatic conditions in the USA as shown by progressively deeper carbonates in soils as a function of progressively wetter regional climates (Jenny and Leonard, 1934) and local orographic climates (Gile, 1977). Generally, a mean annual precipitation of roughly 500 mm (20 inches) is the boundary in the USA above which pedogenic carbonates generally do not form (Birkeland, 1999). However, pedogenic carbonates in soils receiving greater than 500 mm do occur in many regions as relict features i.e., an example of "soil memory" where the carbonates are vestiges of drier climates (Targulian and Goryachkin, 2004).

The SIC-driven threats to agriculture are primarily related to the erosion in croplands with carbonate-rich subsoils (compare Figure 17A and 17B). As erosion proceeds and the depth to carbonate-rich below ground becomes progressively shallower, where the availability of phosphorus and various micro-nutrients such as iron extremely decreases in the rooting zone. Chlorosis due to iron deficiency is very common in calcareous soils (Havlin, 2014). If the SIC exists as a petrocalcic horizon, i.e. a cemented soil layer due to carbonate precipitation, adverse physical soil properties such as reduced water percolation and aeration prevent root penetration, resulting in reduced crop growth and yield. However, the presence of carbonates, as silt-size particles, may impart favourable water-holding properties to plants (Duniway et al., 2010). Regarding CO_2 storage, it can be hypothesized that the exhumed soil carbonate might be a source of atmospheric CO_2 once the carbonate is elevated out of its subsoil biogeochemical environment and exposed to the topsoil with greater dissolution possibility, due to a higher root density and presence of organic acids. A side-by-side comparison of exhumed versus non-eroded soils with petrocalcic horizons showed no statistical difference in CO_2 emissions, at least in the short term of three years (Serna-Pérez et al., 2006).

With increasing global temperatures, increasing desertification can be expected. Of particular concern is the expansion of desert shrublands into semiarid grasslands (Schlesinger et al., 1990). Based on current observations, both water and wind erosion will increase as bare ground between shrubs increases (Monger and Bestelmeyer, 2006). It has been long recognised that increased water erosion causes siltation of local streams and adversely affects water sources (Joel et al., 1937). It has also been recognised that increased wind erosion from desert landscapes has broad regional effects on air quality and intercontinental transfer of particles (Yaalon, 1987).
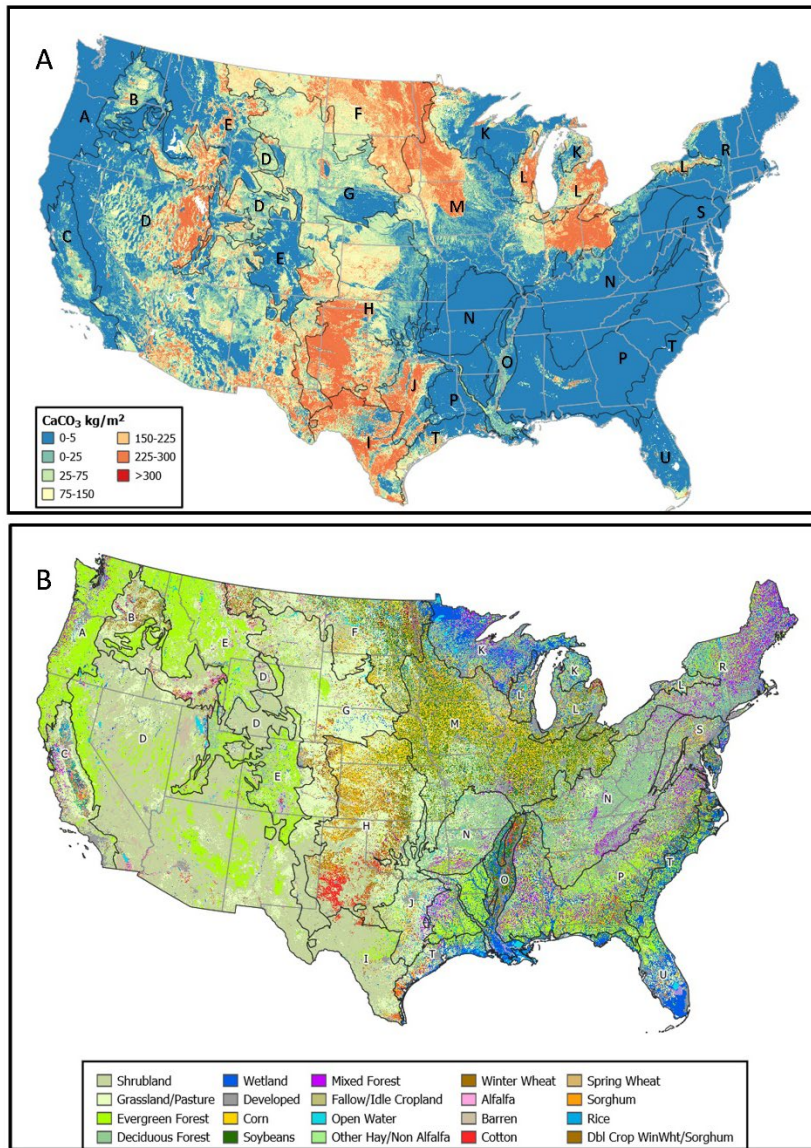
Figure 15 **A)** Soil CaCO₃ distribution in the conterminous United States to a depth of 2 meters. Land Resource Regions are shown as black polygons. **B)** Land use in the conterminous USA based on 2018 data from the USDA National Agricultural Statistics Service. Figures courtesy of Chad Ferguson, US Natural Resources Conservation Service.
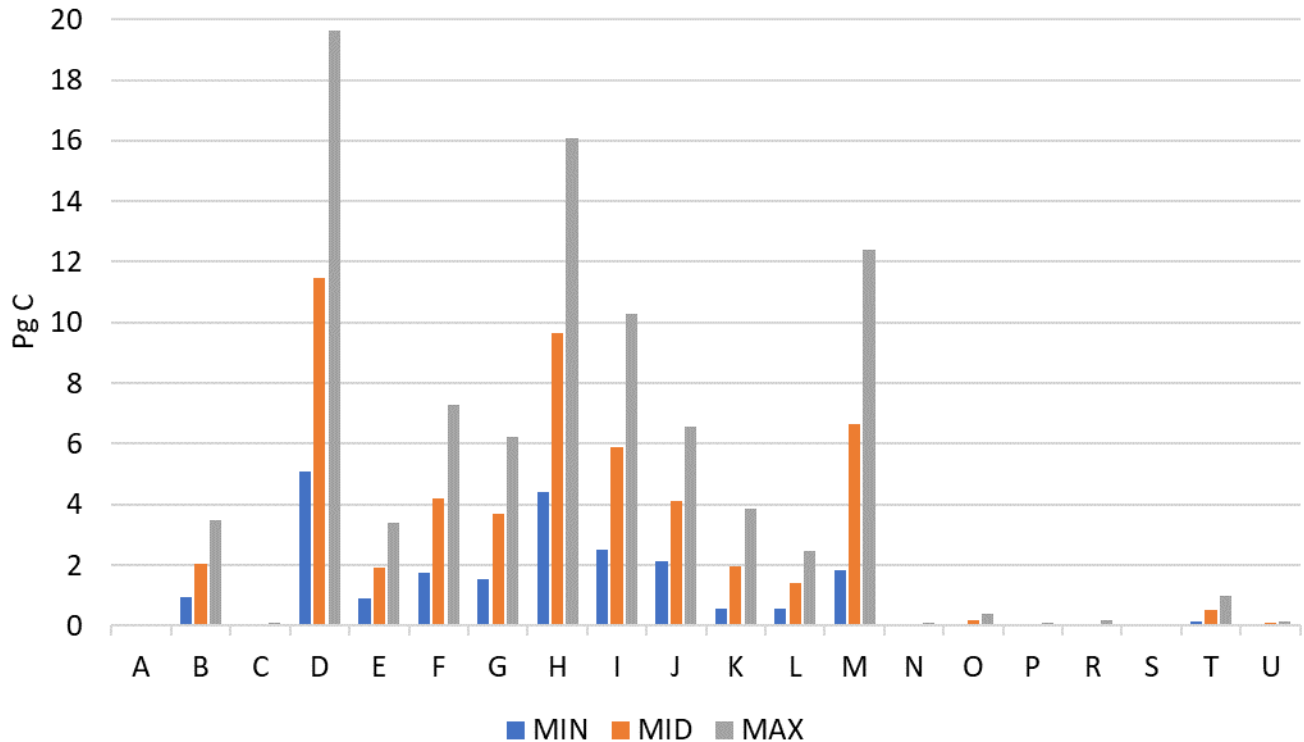
Figure 16. Minimum, median, and maximum amount of soil inorganic carbon within the Land Resource Regions of the conterminous United States (See Fig. 17). Data from Guo et al. (2006a).

A review of digital mapping of SIC stocks

As described in the previous section, many regions still rely on traditional mapping approaches for mapping SIC, delineating soil-landscape units based on the interpretation of remote sensing images and geological maps. Digital soil mapping (DSM) approaches were promoted about two decades ago (McBratney et al., 2003), which have been widely adopted to map SOC concentration and stock throughout the world, have improved global estimates of SOC stocks (Arrouays et al., 2014; Chen et al., 2022). However, digital mapping studies specific to SIC are limited and the global SIC stock estimations are still uncertain as such estimates are based on coarse-scale soil information (Eswaran et al., 1999).

Digital soil mapping helps identify regions with the highest threats, priorities, and drivers of change. In addition, digital maps of SOC and SIC can be used in climate models to assess the sensitivity and feedback to future climate change. Based on DSM within the framework of SCORPAN model (McBratney et al., 2003; Minasny and McBratney, 2016) we surveyed studies on the spatial distribution of SIC concerning

models, covariates and three-dimensional variations. In a comprehensive and systematic literature survey, the following keywords were searched:

"digital soil mapping" and "soil inorganic carbon", "digital soil mapping" and "inorganic carbon", "digital mapping" and "inorganic carbon" , "digital mapping" and "soil inorganic carbon", "digital soil mapping" and "soil calcium carbonate", "digital soil mapping" and "soil carbonate", "inorganic carbon" AND "map" AND "digital" AND "soil", "carbonate" AND "map" AND "digital" AND "soil"

The search results were then manually filtered to get the specific outcomes on digital mapping of SIC. Only studies related to the modelling and mapping or spatial distribution of SIC were included. Studies on SIC using different spectroscopy techniques were also included.

SIC prediction, mapping and modeling

Digital mapping of SIC follows the procedure of SCORPAN framework (McBratney et al., 2003; Minasny and McBratney, 2016) by relating a set of soil forming factors as covariates with SIC content as a continuous soil property.

$$SIC_{x,y} = f\,(S, C, O, R, P, A, N) + e \qquad (8)$$

$SIC_{x,y}$ represents SIC content at geographical position of x (latitude) and y (longitude) as a function of soil position (S), climate (C), organisms (O), including human effects through land use and management, relief (R), parent materials (P), age or time (A) and spatial position (N). The e is the spatially correlated errors. This model links field observations (e.g. carbonate or SIC concentration) to spatial environmental variables captured by proximal or remote sensors via a spatial prediction function f. The model assumes the factors are in a steady state, and the observations should cover the entire range of variation in covariates so that the model can be extrapolated to the whole area. The form of f can be a simple linear model, regression, or machine learning models (Table 2).

Table 2 shows the summary of the literature review on the digital mapping of SIC. The number of publications for SIC digital mapping is significantly smaller than studies on SOC (Lamichhane et al., 2019; Sharififar and Minasny, 2021). Figure 19 shows the distribution of SIC digital mapping studies worldwide using DSM. In the following sections, we will discuss the main factors that can help drive more accurate SIC mapping.
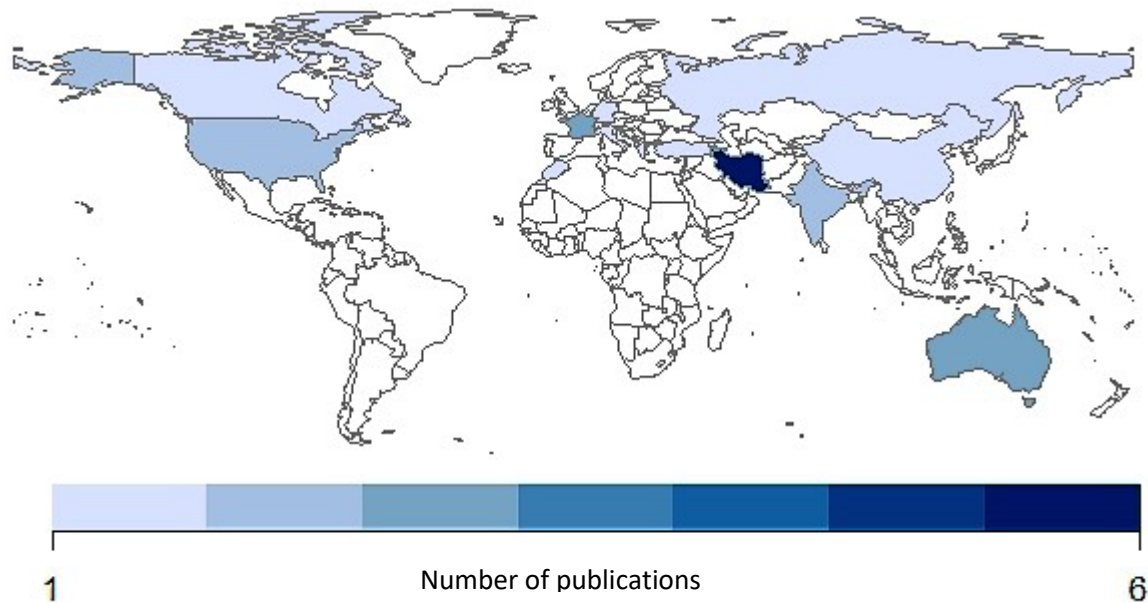
Figure 18. Number of publications on digital mapping of soil inorganic carbon in different countries within the recent decade. [Only studies on SIC mapping based on DSM framework is shown here]

Extent and resolution: SIC has been mapped from field to continental extents at different spatial resolutions. The majority of the studies have mapped SIC at a resolution of ~ 30 m. The resolution of the images corresponds to the mapping extent and utility. For example, the 30 m resolution image may only be suited for regional mapping but cannot detect small pockets of SIC. Some national efforts have been made to map SIC (e.g. in Australia, China, France, and USA), however, many countries still lack data or have not mapped SIC.

Where in the world? Figure 18 shows the publications numbers on SIC digital mapping in different countries. These studies cover various spatial scales from local and regional to national extents. These studies were mainly published in soil science and focused on DSM. In Africa, some parts of Europe and South America, SIC maps are not supplied, possibly because in some of these areas SIC is very low and has not attracted attention as much as in arid and semi-arid regions of the world.

What was mapped? Most of the DSM studies on SIC focused on mapping inorganic carbon concentration or stock. Some studies also mapped SIC occurrence probability (e.g. Filippi et al., 2020), or $CaCO_3$ content (Wilford et al., 2015). Due to the skewness of carbonate distribution, probability of occurrence modelling can help overcome the difficulty of mapping and modelling its spatial variation. The depth to carbonate modelling and mapping could be even more useful for land use planning and soil management, which has not been well explored in the literature.

Inputs: for SIC mapping, most of the studies have used legacy data, often with additional soil sampling. Due to the costs and time limitations, several studies have relied solely on legacy data. In some countries, the soil sampling density was fairly high, although the extent of the study area was small (e.g. Kasraei et al., 2021). In terms of SIC indicators, as explained in the "measuring SIC proximally and remotely" section, different approaches have been used as data input. Using spectral data as inputs for mapping and modelling the spatial distribution of SIC has shown promising predictions, with notably high accuracy of Mid-Infrared (spectral range 4000-400 cm^{-1}), although not for mapping purposes. As an example, the prediction accuracy of SIC using mid-infrared had an $R^2 = 0.97$ in France (Grinand et al., 2012) and $R^2 = 0.99$ in the USA (Seybold et al., 2019). In general, using spectroscopy for sensing SIC and as input for further modelling and mapping can be more cost-effective and less time-consuming than conventional laboratory approaches.

Covariates: the covariates used for the digital mapping of SIC include various variables that directly or indirectly affect the formation or accumulation of SIC and soil inherent spatial variation; among which, climatic factors and lithological variables have been reported as the most important ones that help model and map SIC. Other covariates comprise digital elevation models (DEM) and terrain attributes derived from DEM. The covariates were mainly obtained via satellite images from sources such as ASTER, Landsat, MODIS and Sentinel. Hyperspectral data from remote sensing have been reported as a successful tool for SIC mapping and prediction (e.g., Gomez et al., 2012; Mitran et al., 2021).

Modelling approaches: according to the literature survey, methods of SIC modelling and mapping can be grouped into a few approaches, including:

a) the use of digital soil mapping framework with the help of machine learning and/or geostatistical estimation/simulation by applying soil forming factors as explanatory variables (Minasny and McBratney, 2016). The most used algorithms for SIC digital maps have been random forest, multiple linear regression,

and some other models, including partial least squares regression, artificial neural networks and Cubist (Table 2).

b) chemometric modelling - spectroscopy and proximal soil sensing using Visible Near Infrared (0.4-2.5 µm), Mid-Infrared or integrated methods of spectroscopy with the help of proximal or remote sensors (Gomez et al., 2022; Sepahvand et al., 2019). Spectroscopic methods can be advantageous by providing rapid and cost-effective data with desired spatio-temporal resolution.

c) pedo-climatic and pedogenic knowledge-led mapping; a helpful SIC mapping approach using natural soil and biogeoclimatic characteristics (such as pedocal concept (Marbut, 1935; Salley et al., 2016)) for zoning areas with homogeneous mapping units or sub-zones (Bui et al., 2009; Yang et al., 2017).

d) the use of so-called "taxotransfer rules", which estimate soil properties based on modal characteristics of soil units/taxons (Batjes, 2016).

Unlike SOC, SIC can be difficult to model and map in some areas, as SIC is not contiguously distributed in an area. The measured datasets are often zero-inflated, meaning that many locations have low or no SIC content. To overcome this problem, SIC occurrence can be first predicted, then the stock can be quantified. For example, Filippi et al. (2020) presented such an approach called two-step modelling, where in this case the presence of SIC in the study area was modelled using a random forest model, then used a separate model developed to predict amounts of SIC in those areas where SIC was predicted to be present.

SIC change: Unlike SOC, mapping SIC changes has not been widely explored, possibly because SIC is normally not expected to show notable changes within time. In a study, Song et al. (2022) mapped SIC stock of China using data from a national survey in the 1980s and compared it with data from 2010s. They found an overall decrease in SIC stocks in the top 30 cm (0.11 t C ha^{-1} yr^{-1}). Total SIC stocks have decreased by 9% (1.37 ± 0.37 Pg C). In a semi-arid field in the great plains of the USA, Sherrod et al. (2015) hypothesized that $CaCO_3$ concentration in the soil surface layer is inversely correlated with the change in surface elevation due to erosion and deposition. Using high-resolution DEM, the temporal differences in elevation were related to the change in $CaCO_3$ concentration. This idea should be more explored as a tool for investigating SIC changes.

Validation and uncertainty of SIC maps: the validation approach that most DSM studies have done is based on the data hold-back method, in which a portion of collected data (usually 20-30% of the whole dataset) is used for testing the correctness of the predicted pixels of the produced map. The "leave-one-

out" method can be an efficient alternative when the dataset is small. However, the K-fold cross-validation method can help get a more robust accuracy outcome for skewed data, typical for SIC. In terms of uncertainty quantification, only about 35% of the studies have carried out uncertainty assessment of the digital maps of SIC. There is no report of a specially designed mapping study for SIC along with a designed validation survey – a clear need for the future.

Laboratory analysis, proximal and remote sensing

There are several methods of measuring and detecting the existence of SIC, such as HCl test for carbonates. In the laboratory, the standard methods include the elementar analyzer (i.e. the difference between the measured total C content before and after acidifying the soil sample), calcimetery (i.e. measuring the pressure of CO_2 gas produced following sample acidification), and the titration method to determine the total neutralizing value (TNV) also known as calcium carbonate equivalent (CCE) (Loeppert and Suarez, 1996).

It is important to know the appropriate methods of SIC evaluation, as different soils might require specific approaches (Apesteguia et al., 2018). For example, using calcimetery when different carbonate types are present in soil may lead to underestimating SIC content, especially when only calcium carbonate content is reported as the SIC indicator. Methods for soil carbon measurement with the relative advantages and disadvantages are discussed in detail in Nayak et al. (2019) and Nelson and Sommers (1996).

Indirect measurement using infrared reflectance of soil: Mid-Infrared (MIRS, 2500 -25000 nm, 4000–400 cm^{-1}) and Visible Near Infrared (Vis-NIR, 4-00- 2500 nm, 25000 – 4000 cm^{-1}) reflectance spectroscopy have shown to be able to quantify SIC (Gaffey, 1986; Wijewardane et al., 2018). MIR spectroscopy is based on absorption bands corresponding to fundamental molecular vibrations, while Vis-NIR spectroscopy is based on absorption bands corresponding to weak overtones and combinations of fundamental vibrations (Williams, 1987). Strong fundamental vibrational states related to soil components occur in the MIR between wavelengths 2500 and 25000 nm, including the ones at 700, 880, 1450 and 2510 cm^{-1} related to carbonates (Legodi et al., 2001) (Figure 20a). Several additional bands attributed to carbonates can also be identified at 3000–2900 cm^{-1} due to overtones, and at 2600–2500 and 1830–1760 cm^{-1}, due to combinations of fundamental vibrations (Comstock et al., 2019; Legodi et al., 2001; Nguyen et al., 1991) (Figure 20a). Overtones and combination modes overlap in the Vis-NIR spectral range, and

carbonates have absorption bands at 1.6, 1.7, 2.2, 2.3, and 2.5 µm (Ben-Dor and Banin, 1995) (Figure 20b). As bands are not distinct, estimating carbonate using Vis-NIR is more challenging than MIR.

Several methodologies have been successfully tested to link MIR and Vis-NIR soil spectra to SIC content, such as simple linear regression (SLR) using specific absorbance peaks (Legodi et al., 2001), using the MIR and Vis-NIR domain, respectively, and partial least -squares regression (PLSR) using the entire spectra (Gomez et al., 2022; Wijewardane et al., 2018). Machine learning algorithms such as artificial neural networks, support vector machines, Cubist regression trees, random forest, and deep learning have been successfully applied for estimating SIC concentration (e.g. Dangal et al., 2019; Gruszczyński and Gruszczyński, 2022; Ng et al., 2020).

In-situ approaches for measuring SIC have also been proposed using the Vis-NIR spectrometer, laser induced breakdown spectrometer and inelastic neutron scattering method (Chatterjee et al., 2009). Usually, *in-situ* and *ex-situ* measurement methods can result in somewhat different accuracies. However, the accuracies of these methods can come close to each other when suitable treatments are applied on *ex-situ* methods, as sometimes commonly used for spectroscopic measurements (Leogrande et al., 2021; Wang et al., 2012).

While laboratory Vis-NIR soil spectroscopy may provide correct SIC estimations, Vis-NIR imaging sensors may provide lower accuracies of SIC estimations as these sensors are subject to degradations due to the atmospheric effects, Signal to Noise Ratio of sensors, coarse spatial and spectral resolutions, and soil surface conditions (e.g. Chabrillat et al., 2019; Gomez et al., 2018; Lagacherie et al., 2008). For example, Vaudour et al. (2019) reported R^2 from 0.15 to 0.48 for predicting $CaCO_3$ using Sentinel-2 satellite images in Mediterranean and Temperate contexts. Additionally, Gomez et al. (2008) and Lagacherie et al. (2008) reported R^2 of 0.77 and 0.61, respectively, for SIC prediction based on Vis-NIR hyperspectral imaging sensors (AISA-DUAL and Hymap sensors, respectively).
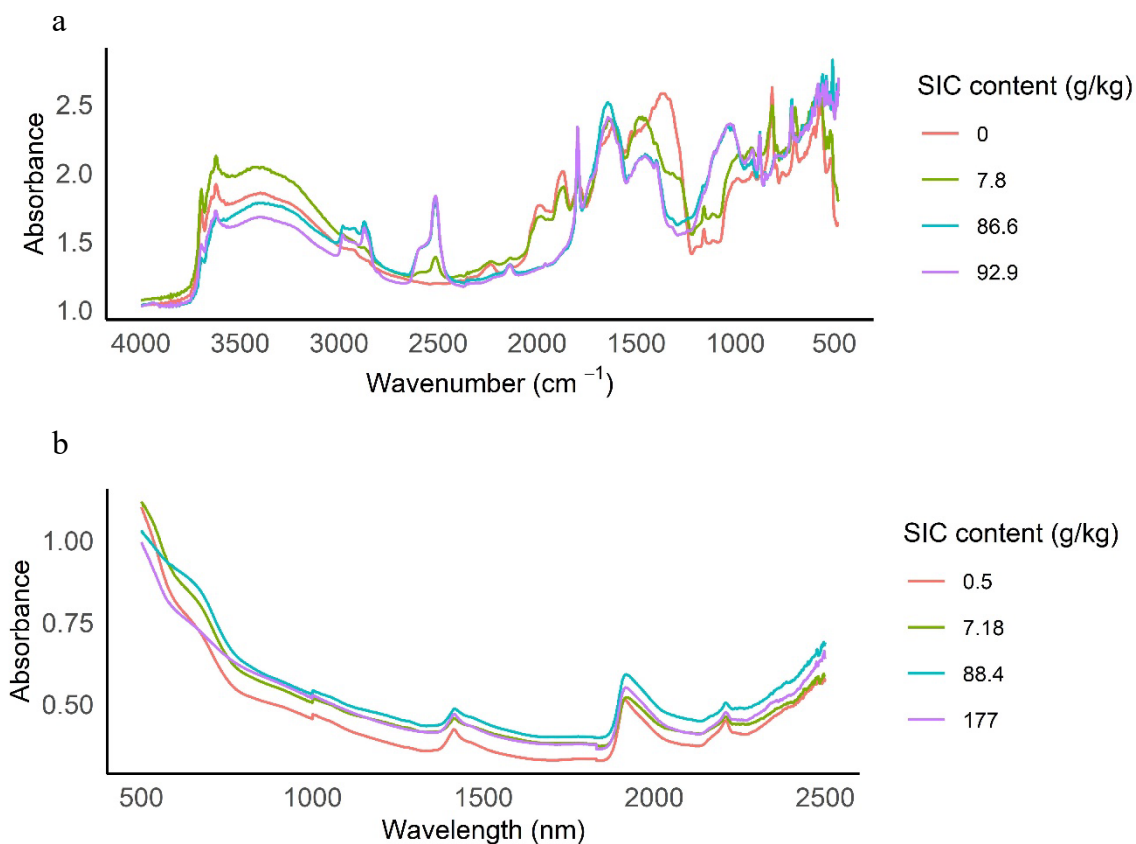
Figure 19. Examples of absorbance spectra of four soil samples collected in Tunisia with varying SIC content using laboratory a) MIR and b) Vis-NIR spectroscopy.

Summary of DSM review

The review of DSM studies shows that SIC can be successfully mapped using the DSM approach, despite the modest number of studies. Some notable gaps in current SIC mapping are:

- The shortage of DSM studies and ignored importance of SIC

Most of the efforts in soil C studies have focused on organic carbon, in terms of its up-to-date data collection, monitoring and mapping. Many countries do not have any updated SIC database, nor do they have a regional or national extent map for it. Furthermore, in the global scale efforts, SOC global maps have been updated in recent years with reasonable spatial resolution, while there is no accurate and updated global map for SIC.

- Challenges in mapping SIC

The DSM of SOC has rapidly progressed worldwide due to the interest in soil carbon sequestration; however, a modest effort was found for DSM of SIC. This could be due to the lack of interest in SIC, but mapping of SIC is more challenging. Many studies successfully mapped topsoil SOC using remote sensing images and other covariates, however, as SIC mostly presents in the deeper depths, covariates that mainly represent surface conditions cannot detect SIC. That also means surveys for SIC needs to sample and measure the whole soil profile. In addition, in some areas, SIC does not exist contiguously, and thus more extensive surveys is needed to first establish its extent.

- The lack of uncertainty assessment of SIC maps

Using the machine-learning algorithms, with the help of "random sampling with/without replacement" and bootstrapping, confidence intervals of predictions in each pixel of SIC map can be evaluated. The literature review showed the lack of exploring stochastic models rather than deterministic models for predicting, modelling and mapping SIC stocks, its depths of accumulation, probability of occurrence and mapping. The application of simulation and stochastic modelling might pave the way for addressing the difficulty in mapping the distribution of highly skewed SIC data. Simulation models can be advantageous as to higher consistency of their outputs, compared to machine learning bootstraps as an alternative uncertainty quantification.

- Monitoring and mapping SIC stock change

While it was thought before that SIC stock is stable over time, there is some evidence that SIC loss can happen within decades, due to anthropogenic interventions. This can affect the sustainability of agricultural production and be more of a significant contributor to climate change than previously thought. Hence, monitoring SIC change is more necessary than once thought before. Multi-source covariates provide geographical information, elevation and optical and radar images which provide better information than a single covariate and can be useful tools for monitoring and mapping SIC temporal changes. Such covariates can help with a better spatial and temporal resolution for monitoring any probable change in SIC stock, mainly in topsoil. As SIC is mainly present in the subsoil, proximal sensors that can penetrate deeper into the soil profile are required for a more detailed assessment.

SIC and SOC relationships

The SIC and SOC are usually considered and mapped separately, while SIC may also control the dynamics of SOC and vice versa. SIC can control SOC by influencing pH and thereby microbial activity, Ca^{2+}-SOC binding and by aggregate formation and stability. Although the direct or indirect role of SIC and Ca^{2+} binding on SOC stabilisation is not entirely well-defined (Rowley et al., 2018), the precipitation of pedogenic carbonates can be a carbon-protecting action, as it can cement aggregates and thus enhance soil aggregation. Three main mechanisms have been suggested to explain the positive impact of SIC on SOC stabilization: (i) aggregation and the occlusion of SOC, (ii) organo-mineral and organo-cation interactions, and (iii) inclusion of SOC within pedogenic or biogenic $CaCO_3$ (Rowley et al., 2018). These mechanisms are mostly linked to the reactivity of the Ca^{2+}, favouring soil aggregation.

Some studies suggested significant protection of SOC within macro-aggregates in calcareous soils in the Mediterranean region (Fernández-Ugalde et al., 2011; Martí-Roura et al., 2019). The structure of macro-aggregates in calcareous soils can be different from carbonate-free soils. These aggregates hold the active precipitation of carbonates (Catoni et al., 2012; Falsone et al., 2010) and favour the stability of SOC. Aggregation can protect SOC from decomposition and favour SOC accumulation and stabilisation (Balesdent et al., 2000). The degree of SOC protection inside aggregates of calcareous soils is yet to be quantified. In addition, Some forms of SIC may also alter SOC decay rates by forming physical coatings around particles or enhanced aggregation (Zornoza et al., 2018).

Conversely, SOC can influence SIC. Carbon for the formation of pedogenic carbonates is generally supplied from CO_2 in the soil solution, because of respiration and decomposition of soil organic matter (Hasinger et al., 2015; Zamanian et al., 2016), demonstrating an interactive relationship between SOC and SIC. Anthropogenic factors can greatly influence this relationship and change the balance between SIC and SOC. For example, liming increases pH and decreases fungal diversity but may increase bacterial diversity leading to SOC mineralization (Xiao et al., 2018).

SIC shows higher spatial variability than SOC, even within given land use types (Stevenson et al., 2005; Wang et al., 2018). The transition from desert to shrublands and crop lands has shown a higher accumulation of both SOC (usually in topsoil) and SIC (mostly in subsoil) (Wang et al., 2018). Positive correlations between SIC and SOC have been reported (Guo et al., 2016; Wang et al., 2015; Guo et al., 2021; Yang et al., 2021; Zhang et al., 2010). The positive relationship has been mostly reported for croplands and in agricultural practices where soil organic matter contributes to SIC formation by providing

carbon source for pedogenic carbonate (Zamanian et al., 2016). On the other hand, a negative relationship between SOC and SIC has been reported for non-agricultural areas (Lu et al., 2020; Raheb et al., 2017; Sharififar et al., 2019a). In such areas, erosion, deposition, and the redistribution of soils are considered the dominant factors affecting SIC and SOC relationship. In addition, biotic and abiotic processes and agricultural practices (e.g. fertilization and liming) can affect the relationship between SIC and SOC, and their abundance at different soil depths.

When assessing the SOC and SIC relationship, land use interaction with pedogenic and geologic phenomena should be considered. Hence, more comprehensive studies with wide-ranging sampling efforts across different soils will help deepen our understanding of the SOC and SIC relationship and balance. This will help find the probable threshold at which SOC and SIC correlation changes in different climatic conditions and land uses. This would also enhance our ability to model a complete picture of soil C and its relation with climate change.

Important factors that need to be considered for SIC and SOC balance and total soil C mapping and modelling are land use change and anthropogenic factors that might change the thresholds where the SIC and SOC relationship changes. As shown in Figure 7, the difference in SIC and SOC stocks is more pronounced in the northern hemisphere than more southerly latitudes. If we can understand the spatial correlation between SIC and SOC, then SOC data/maps (which are much more available than SIC maps) can be used as covariates for SIC mapping.

Human influence and climate-change effects on SIC

There is a general belief that SIC has a millennial residence time and thus has a negligible contribution to global C cycle compared to SOC (Schlesinger, 1985; Zamanian et al., 2016; Zamanian and Kuzyakov, 2022). Therefore, the SIC potential as a regulator of atmospheric CO_2 concentration over human lifetime scales has not been fully explored, especially relative to our understanding of the role of SOC. Nevertheless, SIC, particularly in arid and semiarid regions of the world, can be the main soil C pool, significantly contributing to C sequestration. For example, the amount of sequestered C as SIC in the first and second meter of soils in the conterminous USA, depending on vegetation i.e. shrublands, grasslands and pasture, is about 1.27 to twice the amount of sequestered C as SOC (Guo et al., 2006).

Moreover, the formation of pedogenic carbonates due to the significant contribution of silicate weathering in Canadian prairies, resulted in 1.4 times more C sequestration as SIC than SOC (Landi et al., 2003). In fact, SIC can act as a net sink of atmospheric CO_2 (Lapenis et al., 2008; Laudicina et al., 2013) and help reduce the environmental costs of carbon loss and CO_2 emission across farms (Groshans et al., 2019; Lorenz and Lal, 2022).

Several natural and anthropogenic factors control the contribution of SIC in C sequestration or CO_2 emission. Planting trees and shrubs, especially in arid and semi-arid regions or on unproductive saline and alkaline soils can boost CO_2 in the soil through deeper roots. This will increase CO_2 partial pressure in soil, which may directly result in C sequestration as the H_2CO_3 ion species in soil (Carmi et al., 2019) or lead to silicate weathering, Ca^{2+} release and pedogenic carbonate formation (Haque et al., 2020).

However, there is increasing evidence that the SIC has contributed to CO_2 emissions through human activities such as management practices, especially irrigation, liming and incorporation of legumes into cropping systems (Lal et al., 1999; Shi et al., 2012). Recent studies indicate that the SIC pool progressively becomes more sensitive to anthropogenic acidification and acts as a CO_2 source (Martin, 2017; Monger et al., 2015; Zamanian et al., 2021, 2018; Tao et al., 2022). Intensive agriculture with ammonium-based fertilisation results in soil acidification that accelerates the SIC loss and makes SIC a net source of atmospheric CO_2 (Zamanian et al., 2018).

Irrigation can increase or decrease SIC stocks depending on water amount, water quality and soil conditions. For example, irrigation water can supply Ca^{2+} (and Mg^{2+}) ions to the soil (Bughio et al., 2016), which may subsequently lead to the formation of pedogenic carbonates (de Soto et al., 2019, 2017). The fate of the leached bicarbonate ions through the soil profile can also have different consequences for the C cycle. If the leached bicarbonate ions are re-precipitated at lower soil depths, the process will be carbon neutral. It is still carbon neutral if the carbonate is leached into the groundwater and ends up precipitated in the oceans.

Liming acid soils can have direct and indirect effects on soil carbon. Liming can directly improve acid soils and sequester CO_2 by increasing SOC (Hamilton et al., 2007). Liming can also indirectly affect soil C protection by preserving organic C in soil via, for example, calcium bonding (Eze et al., 2018; Fornara et al., 2011).

As SOC decay and SIC dissolution/precipitation are affected by a complex suite of factors, the global C balance in agricultural soils rich in SIC is still uncertain (Paradelo et al., 2015; Wu et al., 2009). A few

studies have tried to understand and explain the contradiction between the results of the impact of soil management on SIC dynamics (Monger et al., 2015).

Climate and hydrological cycles (i.e. precipitation and evapotranspiration) at local to global scales strongly influence inorganic carbon dynamics and their contribution to atmospheric CO_2 production (Lapenis et al., 2008). For example, scarce rainfall will decrease the dissolution of $CaCO_3$ and the leaching of dissolved Ca^{2+} and Mg^{2+}, which may result in more precipitation of SIC than losses via leaching. The amount of local rainfall determines the depth of the wetting front in the soil profile, coinciding with the presence of SIC in the profile. The rainwater quality can affect the inputs of Ca^{2+} and Mg^{2+} ions to the soil, hence controlling the precipitation of SIC (Wilford et al., 2015). In general, the precipitation to potential evapotranspiration ratio determines SIC dynamics (Tao et al., 2022). Such linkages between the alterations in SIC stocks and climate change further emphasize the importance of DSM in producing an accurate distribution of SIC.

With the CO_2 levels expected to increase to 950 ppm by 2099 (Allen et al., 2018), there is an expectation of increased plant biomass and rhizosphere activity, which could increase soil acidity due to respiration and release of organic acids. Increasing soil acidity tends to dissolve $CaCO_3$ and leads to the leaching of Ca^{2+} and Mg^{2+} ions (Kuzyakov et al., 2019; Raza et al., 2021). An increase in air and soil temperature also increases organismal activity (respiration and release of organic acids), which would intensify the release of CO_2 from carbonate (Ahmad et al., 2015; Chevallier et al., 2016). On the other hand, SIC dissolution by organic acid and respiration can lead to CO_2 sequestration (Appendix; Equation A1). The threshold in which such interactions could lead to net zero emission is still not well investigated. Furthermore, the reactions in the field are more complex than the theories. When SIC is precipitated in deeper depths, the released CO_2 does not necessarily return to the atmosphere but contributes to soil CO_2 (Carmi et al., 2019), which can lead to the dissolution of minerals such as wollastonite ($CaSiO_3$), where its weathering can increase SIC accumulation in soil and CO_2 sequestration (Haque et al., 2020).

Globally, SIC and SOC are being lost due to anthropogenic activity. An estimate of annual losses of SOC due to land cover change is around 1.93 Pg C (Padarian et al., 2021), while estimated annual SIC loss due to fertilization is about 7.5 Tg C (Zamanian et al., 2021). The potential of SIC as a source of CO_2 is even larger when we consider the contribution of liming. Neutralization of agricultural lime i.e. a mixture of $CaCO_3$ and $MgCO_3$, which is added to acid soils to optimize the pH value for crop production, further releases 273 Tg C per year (Zamanian et al., 2021).

With climate change, alterations in soil C stocks become more important. While SOC stocks can be increased through better management, SIC losses are irreversible, with no expected equilibrium as long as fertilization is applied (Raza et al., 2021). Furthermore, SOC stability, at least in calcareous soils, can be controlled by SIC (Ahmad et al., 2015; Fornara et al., 2011). Nevertheless, the dynamics of SIC because of future climate change and land management are generally overlooked. Current climate-change scenarios indicate that about 7% of Australian land will experience increased drying until 2050. About 6.5 million km^2 are foreseen to suffer from 10% decline in surface soil moisture in the driest decade of 2030 to 2040 (Guglielmo et al., 2021). Despite potential consequences of such climatic changes for alteration in SIC stocks, they have been so far unaccounted for predicting the dynamics of SIC. Because the focus has almost always been to study the dynamics of SOC in response to climate change and global warming. Similarly, the current and future land-use changes that result in acidification and/or changes in soil hydrology will also affect the persistence of SIC and its losses. Thus, global efforts to mitigate climate change through land management and soil C sequestration should also consider SIC.

Concluding remarks

Soil carbon is regarded as a key negative emission technology. This C sequestration potential of soils will be compromised if SIC is lost through agricultural practices such as irrigation and fertilization, which are usually employed for organic C sequestration. We need to account for both SOC and SIC to build a complete picture of the soil C cycle. In addition, understanding the interaction of both C forms helps build resilient soils to global changes. Currently, the spatial information on SIC distribution and stock is relatively scarce and digital soil mapping efforts to address this are modest. Furthermore, we do not have a complete joined-up soil C model that explicitly accounts for all sources and sinks of soil carbon.

This review showed that many aspects of SIC in DSM and soil C studies have been so far ignored and that SIC has a crucial role in climate regulation. SIC and SOC need to be integrated into DSM and integrate SIC into a SOC modelling framework. With the help of new mechanistic models that consider both SIC and SOC, we can comprehensively monitor and predict soil carbon changes over decadal scales and at local to global spatial scales. This is of high importance to secure our soil resources against the negative impacts of global changes.

Acknowledgments

Appendix

CO₂ emission and sequestration reactions

To understand the net contribution of SIC in atmospheric CO_2, the fate of the dissolved Ca ions should be considered. The incomplete leaching results in the accumulation of dissolved Ca ions in lower soil depths, which could lead to $CaCO_3$ re-precipitation and CO_2 emission. This reaction frequently occurs in arid and semi-arid regions, where evapotranspiration is higher than precipitation and roots take water up from deeper depths. Thus, under natural conditions (Equation A1), $CaCO_3$ dissolution and re-precipitation will be neither a sink nor a source of atmospheric CO_2 (Zamanian et al., 2018), although, it provides a temporary sink of C as long as HCO_3^- stays in solution (Equation A1) (Monger et al., 2015; Zamanian et al., 2021). $CaCO_3$ dissolution leads to C sequestration (Equation A1 goes to right), while $CaCO_3$ re-precipitation results in CO_2 release (Equation A1 goes to the left) (Zamanian and Kuzyakov, 2022):

$$CaCO_3 + CO_2 + H_2O \leftrightarrow Ca^{2+} + HCO_3^- + HCO_3^- \qquad (A1)$$

(C in red is carbonate sourced C, and C in blue is CO_2 sourced C)

It should be noted that lithology and water availability can determine the amount of C flux from soils (Hartmann, 2009). In this regard, the rock and mineral type matter, as silicate minerals can have higher potential to sequester atmospheric CO_2 (Equations A2 & A3), compared to carbonate minerals. The following reaction of olivine shows the capacity of silicates as a net sink for up to 50% of the consumed atmospheric CO_2:

$$Mg_2SiO4 + 4CO_2 + 4H_2O \rightarrow 2Mg^{2+} + 4HCO_3^- + H_4SiO_4 \rightarrow 2MgCO_3\downarrow + SiO_2\downarrow + 2CO_2\uparrow + 2H_2O \quad (A2)$$

For albite, the net sink will be 100% of the consumed atmospheric CO_2:

$$2NaAlSi_3O_8 + 2CO_2 + 11H_2O \rightarrow Al_2Si_2O_5(OH)_4 + 2Na^+ + 2HCO_3^- + 4H_4SiO_4 \rightarrow 2Na^+ + 2HCO_3^- + SiO_2\downarrow \quad (A3)$$
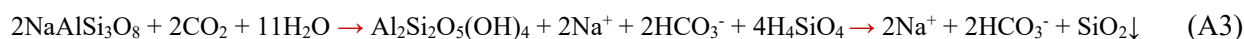
Weathering of silicates (e.g. as in Equation A4) may lead to the release of Ca and C sequestration via $CaCO_3$ precipitation (Cueva et al., 2019; Mikhailova and Post, 2006; Wang et al., 2014).

$$CaSiO_3(s) + 2CO_2 + 3H_2O \rightarrow Ca^{2+}(aq) + 2HCO_3^-(aq) + H_4SiO_4 \rightarrow CaCO_3(s) + CO_2\uparrow + 3H_2O + SiO_2 \quad (A4)$$
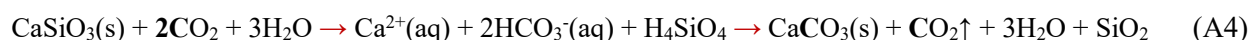
Weathering of silicates is generally considered a carbon sequestering process (Equation A4) (Beerling et al., 2018; Cipolla et al., 2021a, 2021b). Whilst, anthropogenic interventions such as fertilisation of calcareous soils (Equation A5) and liming of acid soils (Equation 14) lead to CO_2 emission out of SIC

(Azeem et al., 2022; Raza et al., 2021; Xie et al., 2021; Zamanian et al., 2018; Zamanian and Kuzyakov, 2019).

For example, the following reactions of urea ($CO(NH_2)_2$) shows the release of CO_2. Note that, nitrate is kept in the formula to show the source of acidity:

$$CO(NH_2)_2 + H_2O \rightarrow 2NH_3 + CO_2\uparrow$$

$$NH_3 + H_2O \rightarrow NH_4^+ + OH^-$$

$$NH_4^+ + OH^- + 2O_2 \rightarrow NO_3^- + H^+ + 2H_2O$$

$$CaCO_3 + 2NO_3^- + 2H^+ \rightarrow Ca^{2+} + 2NO_3^- + CO_2\uparrow + H_2O \qquad (A5)$$
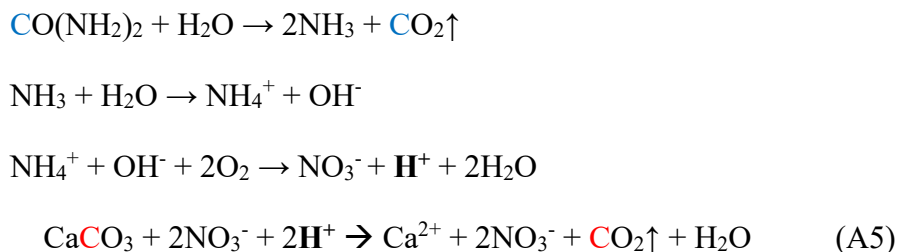
And the effect of liming is illustrated in the following:

$$CaCO_3 + H_2\text{-}X \rightarrow Ca\text{-}X + H_2O + CO_2\uparrow \qquad (A6)$$
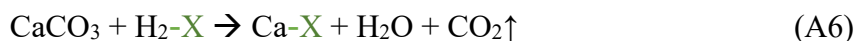
where, X is an exchangeable site such as soil clay particles.

Table 1. Summary of studies on controlling factors of SIC

Country	Climate	Controlling factors (the ones in bold were found as the most important)	IC and OC relationship	Method of assessment	Max soil depth (cm)	Reference
China	Semi-arid continental	Afforestation	NA	Statistical comparison	100	(Chang et al., 2012)
Australia	Sampling location: humid subtropical with a semi-arid influence [in Wagga Wagga, NSW]	Liming and wheat plant effects on DIC leaching and C-efflux	NA	Analysis of variance, time effect, Tukey's HSD and Student t-test	25	(Ahmad et al., 2013)
China	Arid and semi-arid continental monsoon	Land use and soil type	NA	Comparison of SIC densities in different sites	100	(Tan et al., 2014)
China	Temperate semi-arid continental monsoon	Desertification stages	Positive	Analysis of variance, linear regression	30	(An et al., 2019a)

Meta-analysis of 29 studies	Arid and semi-arid regions	**Land use change** & indirect factors: pH, MAT, MAP, SOC, soil sampling depth	In some cases positive	Response ration & correlation	100	(An et al., 2019b)
Spain	Typical Mediterranean continental	Land use (cropland & rangeland), soil redistribution	In rangeland: negative In cropland: positive (neither was significant)	Pearson correlation, least squares of the general linear models	55	(Gaspar et al., 2019)
Iran	Semi-arid	Soil basal respiration, dehydrogenase enzyme activity, bacteria population + **physicochemical properties group**	Negative	Pearson correlation, Variation partitioning analysis	15	(Sharififar et al., 2019)
China	Semi-arid	Erosion (sediment transport and its influencing factors: raindrop size, **PSD**[3], **runoff rate**, inflow rate)	Negative	Boosted regression tree & Pearson correlation	20	(Wang et al., 2019)

China	Subtropical monsoon	**Reclamation duration**, land use change, physio-chemical properties such as **CaO**, **Fe & Al oxides, C:N, texture**	NA	Random forest model	20	(Zhang et al., 2019)
China	Arid to semi-arid	MAT, MAP, geographic position (latitude, longitude, altitude), soil type, pH, **moisture**, land use, climate, **OC**	Negative in all depth layers	Structural equation modeling	100	(Zhao et al., 2019)
Cypress	Subtropical Mediterranean and semi-arid	**lithology**, land use/cover, major and trace elements, SOC, climatic factors	NA[2]	Spatial correlation using variography	20	(Zissimos et al., 2019)
China	Cold semi-arid	MAT, **MAP**, **pH**, total N, total C, C:N, soil water content, DON, TDN, SOC:SIC, NH_4^+-N, NO_3-N	Negative	Generalized linear model	70	(Du and Gao, 2020)
Spain	Sub-humid Mediterranean mountain agrosystem	Runoff/water erosion: land use & vegetation cover; curvature & flow accumulation: all important	Na	Analysis of variance, ^{137}Cs inventories, perceptual modeling, Kruskal-Wallis test	5	(Gaspar et al., 2020)

China	Temperate Semi-arid continental monsoon	Soil erosion types, SOC	At erosional sites: negative At depositional sites: positive	Partial least squares regression & analysis of variance	600	(Tong et al., 2020)
Meta-analysis	Polar, temperate, sub-tropical, tropical	MAT, MAP, **land use, basin surface area, morphology of the river basins**: on dissolved IC transitioning by water	NA	Mata-analysis; correlation	-	(Chaplot and Mutema, 2021)
Italy	Semi-arid Mediterranean	Factors affecting IC accumulation and CO_2 sequestration: Relief, distance from gypsum outcrops, parent material, Ca^{2+} from gypsum	NA	Kinetic and thermodynamic geochemical model, ion activity, log Q/K ratio, Gibbs free energies	150	(Laudicina et al., 2021)
China	Semi-arid continental monsoon	Revegetation: enhancing **N**, available K, CEC, **clay, Ca^{2+}, Mg^{2+}**	Positive	Analysis of variance, linear regression, Redundancy analysis	20	(Li et al., 2021)

South Africa	Arid and semi-arid	Grazing intensity, soil particle size distribution	NA	Analysis of variance, Tukey's HSD test	5	(Loke et al., 2021)
Iran	Semi-arid	Elevation, slope, stream power index, **topographic wetness index, alkaline cations**	Negative	Analysis of variance, stepwise multiple regression, Pearson correlation	20	(Mohseni and Salar, 2021)
China	Subtropical to warm temperate monsoon	**particle size**, pH, salinity, **N**, P, S	Positive	Partial least squares regression	3	(Yang et al., 2021)

Note: The review of "SIC controlling factors" is not a comprehensive survey, but important examples from different countries.

Table 2. Summary of studies on the digital mapping of soil inorganic carbon.

Study area	Extent	Fitting method	Covariates	Accuracy (R^2)	Max Soil depth (cm)	Spatial resolution (meter)	No of samples	Uncertainty: confidence of prediction (Yes/No)	Reference
Australia	4.6 km^2	Partial least squares regression, regression rule model, zonal statistic for class mapping	Mid infrared spectroscopy, **DEM**, secondary terrain attributes: **EM31 EC$_a$, radiometric thorium**	RMSE=4.21 , Mean observed value=8.92	100	5	60	No	(Miklos et al., 2010)
France	National	Partial least square regression	-	0.97	30	16 km	2086	No	(Grinand et al., 2012)

		and Mid infrared spectroscopy							
France	24.6 km^2	Airborne Vis-NIR spectroscopy by PLSR	HyMap hyperspectral image	0.76 (for CaCO$_3$)[1]	5	5	95	No	(Gomez et al., 2012)
Turkey	4949.39 km^2	Landsat 7 ETM+, Linear regression	Short wave infrared band of Landsat 7	~ 0.71	20	30	164	No	(Dogan and Kılıç, 2013)
Morocco	15000 km^2	Multiple linear regression; x-ray diffraction	ASTER satellite data, material identification and characterization algorithm	0.42 (CaCO$_3$)	Not defined	90	73	No	(Mulder et al., 2013)
France	550,000 km^2	Linear mixed	Geology(parent material)	(SIC concentratio	30	2.5 km	~ 2000	Yes	(Marchant et al., 2015)

		model & kriging		n) AIK: 1532.3, prediction error : 0.43					
Australia	National 7.7 Mkm^2	Decision tree based on piecewise linear regression	Geology, **surface geochemistry**, soils, climate, vegetation, terrain, multispectral satellite data	0.50	0-10 & 60-80	90	1311 (calcium carbonate)	Yes	(Wilford et al., 2015)
Iran	88 km^2	**Artificial neural network**, boosted regression tree, **generalized linear**	**Terrain attributes**, remote sensing indices, geology map, existing soil map,	0.25 Calcium carbonate equivalent	30	50	120	No	(Mosleh et al., 2016)

		model, multiple linear regression	geomorphology map						
India	National 3,000,000 km²	RF	Remote sensing, climatic, land cover, rock type, soil type, NDVI, irrigation status	0.86	100	250	1198	No	(Sreenivas et al., 2016)
Iran	12.25 km²	**ANN**, gene expression programming, multivariate linear regression	Terrain attributes, Landsat 7 images, **vegetation features**	0.72 (Calcium carbonate equivalent)	10	30	137	No	(Mahmoudabadi et al., 2017)
Germany	3600 km²	Partial least square	Diffuse reflectance	Root mean square	30	200	1170	No	(Mirzaeitalarposhti et al., 2017)

		regression + ordinary kriging for mapping	infrared Fourier transform mid-infrared spectroscopy	standardized error = ~1					
China	30,000 km^2	RF with the help of pedogenic knowledge	Climate data, terrain attributes, Landsat 5 and its derivatives, **latitude & longitude positions**	LCC: 0.86	100	90	99	No	(Yang et al., 2017)
Greece	112.6 km^2	Artificial neural network	Landsat 8, Sentinel 2, Field proximal sensing	Calcium carbonates: 0.60-0.74	20	30	30	No	(Alexakis et al., 2019)

Europe	Continental	Gaussian process regression	MODIS data, DEM, climatic data	Calcium carbonates: 0.61	20	250	21682	Yes	(Ballabio et al., 2019)
USA	150000 km²	Classification and Regression Tree, Bagged Regression Tree, Boosted Regression Tree, **RF**, **Support Vector Machine**, Partial Least Square Regression, Regression Kriging,	Most important: lithology & climatic factors	Total carbon: 0.72	20	30	1014	No	(Keskin et al., 2019)

		Ordinary Kriging							
Italy	17200 km²	Multinomial logistic regression (for mapping classes of CaCO₃)	DEM (**depth of valleys**, **flow accumulation**), **geology**, pedoclimate-temperature, soil moisture, morphometric parameters, Landsat 8 images (& spectral bands indices)	Cohen's Kappa = 0.58 (CaCO₃)	Profile samples; but the exact depth was Not defined	30	1510	No	(Piccini et al., 2019)
USA	National	Mid-infrared spectroscopy + partial	-	0.99	-	-	36000	No	(Seybold et al., 2019)

		least squares							
Iran	860 km²	**Cubist**, random forest, regression tree, multiple linear regression	DEM, Landsat Enhanced Thematic Mapper data; best: ratio vegetation index & Landsat ETM band 4	0.30	30	30	334	No	(Zeraatpisheh et al., 2019)
Cypress	9250 km²	IDW, Kriging	Parent material as controlling factor	-	70	-	3219	No	(Zissimos et al., 2019)
Iran	567 km²	RF and **Cubist**	Terrain indices and **multi-temporal satellite**	0.70	30	30	142	Yes	(Fathololoumi et al., 2020)

			images (Landsat 8)						
Australia	2650 km²	RF, **combined model**	Land use, NDVI, Topographic data, geology, gamma radiometrics	LCC: 0.40	50	30	154	No	(Filippi et al., 2020)
Canada	95 km²	Random forest, Cubist, SVM[3], **K-nearest neighbors**	Topographic variables, biogeoclimatic subzones, bedrock geology	0.05-0.10	0-145	3	171	Yes	(Kasraei et al., 2021)
Russia	0.35 km²	Process-based modeling: subordination of soil processes to	Topography data, climate data, **hydrological model** (as a landscape	Accuracy[2]: 64%	1-6m	-	157	Yes	(Lozbenev et al., 2021)

		landscape processes and nesting of the soil system into the landscape	process element)						
Azerbaij an	4.23 km^2	Universal kriging, **Random forest kriging**	Terrain attributes, spectral indices, Pl´eiades-1 satellite data	RMSE = 2.00 (CaCO$_3$)	15	12.5	115	Yes	(Mammadov et al., 2021)
India	89 km^2	Linear regression	Airborne hyperspectral Vis-NIR spectroscopy	0.58 (CaCO$_3$)	Not defined	4	24	Yes	(Mitran et al., 2021)
Middle east	3338000 km^2	Random forest (with the help of Google	30 covariates including: soil, climate, relief, parent	0.54 (CaCO$_3$)	20	30	5000	Yes	(Poppiel et al., 2021)

		Earth Engine)	material and age features: most important ones: **annual precipitation and temperature, elevation**						

[1]calcium carbonate is considered as inorganic carbon, but might be an underestimation of the whole soil inorganic carbon as it does not include all carbonates.

[2] accuracy of prediction for Calcium carbonate depth

[3]support vector machine

References

Aburto, F., Hernández, C., Pfeiffer, M., Casanova, M., Luzio, W., 2008. Northern field-guide. The International Conference and Field Workshop on Soil Classification. Soil: A Work of Art of the Nature. Universidad de Chile, Santiago.

Ahmad, W., Singh, B., Dalal, R.C., Dijkstra, F.A., 2015. Carbon dynamics from carbonate dissolution in Australian agricultural soils. Soil Res. 53, 144–153.

Ahmad, W., Singh, B., Dijkstra, F.A., Dalal, R.C., 2013. Inorganic and organic carbon dynamics in a limed acid soil are mediated by plants. Soil Biol. Biochem. 57, 549–555.

Alexakis, D.D., Tapoglou, E., Vozinaki, A.-E.K., Tsanis, I.K., 2019. Integrated use of satellite remote sensing, artificial neural networks, field spectroscopy, and GIS in estimating crucial soil parameters in terms of soil erosion. Remote Sens. 11, 1106.

Allen, M., Babiker, M., Chen, Y., de Coninck, H.C., 2018. IPCC SR15: Summary for policymakers, in: IPCC Special Report Global Warming of 1.5 °C. Intergovernmental Panel on Climate Change.

An, H., Li, Q.-L., Yan, X., Wu, X.-Z., Liu, R., Fang, Y., 2019a. Desertification control on soil inorganic and organic carbon accumulation in the topsoil of desert grassland in Ningxia, northwest China. Ecol. Eng. 127, 348–355.

An, H., Wu, X., Zhang, Y., Tang, Z., 2019b. Effects of land-use change on soil inorganic carbon: A meta-analysis. Geoderma 353, 273–282.

Apesteguia, M., Plante, A.F., Virto, I., 2018. Methods assessment for organic and inorganic carbon quantification in calcareous soils of the Mediterranean region. Geoderma Reg. 12, 39–48.

Arkley, R.J., 1963. Calculation of carbonate and water movement in soil from climatic data. Soil Sci. 96, 239–248.

Arrouays, D., Jolivet, C., Boulonne, L., Bodineau, G., Saby, N., Grolleau, E., 2002. A new projection in France: a multi-institutional soil quality monitoring network. Comptes Rendus l'Académie d'Agriculture Fr.

Arrouays, D., McKenzie, N., de Forges, A.R., Hempel, J., McBratney, A.B., 2014.

GlobalSoilMap: basis of the global spatial soil information system. CRC press.

Azeem, M., Raza, S., Li, G., Smith, P., Zhu, Y.-G., 2022. Soil inorganic carbon sequestration through alkalinity regeneration using biologically induced weathering of rock powder and biochar. Soil Ecol. Lett. 1–14.

Balesdent, J., Chenu, C., Balabane, M., 2000. Relationship of soil organic matter dynamics to physical protection and tillage. Soil tillage Res. 53, 215–230.

Ballabio, C., Lugato, E., Fernández-Ugalde, O., Orgiazzi, A., Jones, A., Borrelli, P., Montanarella, L., Panagos, P., 2019. Mapping LUCAS topsoil chemical properties at European scale using Gaussian process regression. Geoderma 355, 113912.

Batjes, N.H., 2016. Harmonized soil property values for broad-scale modelling (WISE30sec) with estimates of global soil carbon stocks. Geoderma 269, 61–68.

Batjes, N.H., 2014. Total carbon and nitrogen in the soils of the world. Eur. J. Soil Sci. 65, 10–21.

Batjes, N.H., 2004. Soil carbon stocks and projected changes according to land use and management: a case study for Kenya. Soil Use Manag. 20, 350–356.

Beerling, D.J., Kantzas, E.P., Lomas, M.R., Wade, P., Eufrasio, R.M., Renforth, P., Sarkar, B., Andrews, M.G., James, R.H., Pearce, C.R., 2020. Potential for large-scale CO2 removal via enhanced rock weathering with croplands. Nature 583, 242–248.

Ben-Dor, E., Banin, A., 1995. Near-infrared analysis as a rapid method to simultaneously evaluate several soil properties. Soil Sci. Soc. Am. J. 59, 364–372.

Birkeland, P.W., 1999. Soils and Geomorphology, 430 New York: Oxford University Press.

Bockheim, J., Coronato, A., Rabassa, J., Ercolano, B., Ponce, J., 2009. Relict sand wedges in southern Patagonia and their stratigraphic and paleo-environmental significance. Quat. Sci. Rev. 28, 1188–1199.

Bockheim, J.G., Douglass, D.C., 2006. Origin and significance of calcium carbonate in soils of southwestern Patagonia. Geoderma 136, 751–762.

Brahim, N., Bernoux, M., Gallali, T., 2012. Pedotransfer functions to estimate soil bulk density for Northern Africa: Tunisia case. J. Arid Environ. 81, 77–83.

Brus, D.J., Saby, N.P.A., 2016. Approximating the variance of estimated means for systematic random sampling, illustrated with data of the French Soil Monitoring Network. Geoderma 279, 77–86.

Bughio, M.A., Wang, P., Meng, F., Chen, Q., Li, J., Shaikh, T.A., 2017. Neoformation of pedogenic carbonate and conservation of lithogenic carbonate by farming practices and their contribution to carbon sequestration in soil. J. Plant Nutr. Soil Sci. 180, 454–463.

Bughio, M.A., Wang, P., Meng, F., Qing, C., Kuzyakov, Y., Wang, X., Junejo, S.A., 2016. Neoformation of pedogenic carbonates by irrigation and fertilization and their contribution to carbon sequestration in soil. Geoderma 262, 12–19.

Bui, E., Henderson, B., Viergever, K., 2009. Using knowledge discovery with data mining from the Australian Soil Resource Information System database to inform soil carbon mapping in Australia. Global Biogeochem. Cycles 23.

Cardinael, R., Chevallier, T., Guenet, B., Girardin, C., Cozzi, T., Pouteau, V., Chenu, C., 2020. Organic carbon decomposition rates with depth and contribution of inorganic carbon to CO_2 emissions under a Mediterranean agroforestry system. Eur. J. Soil Sci. 71, 909–923.

Carmi, I., Kronfeld, J., Moinester, M., 2019. Sequestration of atmospheric carbon dioxide as inorganic carbon in the unsaturated zone under semi-arid forests. Catena 173, 93–98.

Catoni, M., Falsone, G., Bonifacio, E., 2012. Assessing the origin of carbonates in a complex soil with a suite of analytical methods. Geoderma 175, 47–57.

Chabrillat, S., Ben-Dor, E., Cierniewski, J., Gomez, C., Schmid, T., van Wesemael, B., 2019. Imaging spectroscopy for soil mapping and monitoring. Surv. Geophys. 40, 361–399.

Chang, R., Fu, B., Liu, G., Wang, S., Yao, X., 2012. The effects of afforestation on soil organic and inorganic carbon: A case study of the Loess Plateau of China. Catena 95, 145–152.

Chatterjee, A., Lal, R., Wielopolski, L., Martin, M.Z., Ebinger, M.H., 2009. Evaluation of different soil carbon determination methods. Crit. Rev. Plant Sci. 28, 164–178.

Chen, S., Arrouays, D., Mulder, V.L., Poggio, L., Minasny, B., Roudier, P., Libohova, Z., Lagacherie, P., Shi, Z., Hannam, J., 2022. Digital mapping of GlobalSoilMap soil properties at a broad scale: A review. Geoderma 409, 115567.

Chevallier, T., Cournac, L., Hamdi, S., Gallali, T., Bernoux, M., 2016. Temperature dependence of CO2 emissions rates and isotopic signature from a calcareous soil. J. Arid Environ. 135, 132–139.

Chevallier, T., Gomez, C., Moulin, P., Bouferra, I., Hmaidi, K., Arrouays, D., Jolivet, C., Barthès, B., 2020. Prediction of soil organic and inorganic carbon concentrations in Tunisian samples by mid-infrared reflectance spectroscopy using a French national library, in: EGU General Assembly Conference Abstracts. p. 13092.

Chplot, V., Mutema, M., 2021. Sources and main controls of dissolved organic and inorganic carbon in river basins: a worldwide meta-analysis. J. Hydrol. 126941.

Cipolla, G., Calabrese, S., Noto, L.V., Porporato, A., 2021a. The role of hydrology on enhanced weathering for carbon sequestration I. Modeling rock-dissolution reactions coupled to plant, soil moisture, and carbon dynamics. Adv. Water Resour. 103934.

Cipolla, G., Calabrese, S., Noto, L.V., Porporato, A., 2021b. The role of hydrology on enhanced weathering for carbon sequestration II. From hydroclimatic scenarios to carbon-sequestration efficiencies. Adv. Water Resour. 103949.

CIREN., 1996a. Estudio Agrológico Región Metropolitana. Descripciones de suelos, materiales y símbolos. Publicación No 115. Centro de Información de Recursos Naturales (CIREN), Santiago, Chile.

CIREN., 1996b. Estudio Agrológico VI Región. Descripciones de suelos, materiales y símbolos. Publicación No 114. Centro de Información de Recursos Naturales (CIREN), Santiago, Chile.

CIREN., 1997. Estudio Agrológico VII Región. Descripciones de suelos, materiales y símbolos. Publicación No 117. Centro de Información de Recursos Naturales (CIREN), Santiago, Chile.

Comstock, J.P., Sherpa, S.R., Ferguson, R., Bailey, S., Beem-Miller, J.P., Lin, F., Lehmann, J., Wolfe, D.W., 2019. Carbonate determination in soils by mid-IR spectroscopy with regional and continental scale models. PLoS One 14, e0210235.

Cromack Jr, K., Sollins, P., Graustein, W.C., Speidel, K., Todd, A.W., Spycher, G., Li, C.Y., Todd, R.L., 1979. Calcium oxalate accumulation and soil weathering in mats of the

hypogeous fungus Hysterangium crassum. Soil Biol. Biochem. 11, 463–468.

Cueva, A., Volkmann, T.H.M., van Haren, J., Troch, P.A., Meredith, L.K., 2019. Reconciling negative soil CO2 fluxes: Insights from a large-scale experimental hillslope. Soil Syst. 3, 10.

D'Avello, T.P., Waltman, W.J., Waltman, S.W., Thompson, J.A., Brennan, J., 2019. Revisiting the Pedocal/Pedalfer boundary and Soil Moisture Regimes using the javaNewhall simulation model and PRISM data. Geoderma 353, 125–132.

D'Orazio, M., 2003. Estimating the variance of the sample mean in two-dimensional systematic sampling. J. Agric. Biol. Environ. Stat. 8, 280–295.

Dangal, S.R.S., Sanderman, J., Wills, S., Ramirez-Lopez, L., 2019. Accurate and precise prediction of soil properties from a large mid-infrared spectral library. Soil Syst. 3, 11.

Darwish, T., Atallah, T., Fadel, A., 2018. Challenges of soil carbon sequestration in the NENA region. Soil 4, 225–235.

de Soto, I.S., Virto, I., Barré, P., Enrique, A., 2019. Effect of irrigation on carbonate dynamics in a calcareous soil using isotopic determinations. Spanish J. Soil Sci. 9.

de Soto, I.S., Virto, I., Barré, P., Fernández-Ugalde, O., Antón, R., Martínez, I., Chaduteau, C., Enrique, A., Bescansa, P., 2017. A model for field-based evidences of the impact of irrigation on carbonates in the tilled layer of semi-arid Mediterranean soils. Geoderma 297, 48–60.

Díaz Vial, C., Avilés, C., Roberts, R.C., 1960. Los grandes grupos de suelos de la Provincia de Magallanes.

Ditzler, C., Scheffe, K., Monger, H.C., 2017. USDA Handbook 18. Gov. Print. Off. Washington, DC, USA.

Díaz-Hernández, J.L., Fernández, E.B., González, J.L., 2003. Organic and inorganic carbon in soils of semiarid regions: a case study from the Guadix–Baza basin (Southeast Spain). Geoderma 114, 65–80.

Dogan, H.M., Kılıç, O.M., 2013. Modelling and mapping some soil surface properties of Central Kelkit Basin in Turkey by using Landsat-7 ETM+ images. Int. J. Remote Sens. 34, 5623–

5640.

Douglass, D.C., Bockheim, J.G., 2006. Soil-forming rates and processes on Quaternary moraines near Lago Buenos Aires, Argentina. Quat. Res. 65, 293–307.

Du, C., Gao, Y., 2020. Opposite patterns of soil organic and inorganic carbon along a climate gradient in the alpine steppe of northern Tibetan Plateau. Catena 186, 104366.

Duniway, M.C., Herrick, J.E., Monger, H.C., 2010. Spatial and temporal variability of plant-available water in calcium carbonate-cemented soils and consequences for arid ecosystem resilience. Oecologia 163, 215–226.

Ebeling, A., Oerter, E., Valley, J.W., Amundson, R., 2016. Relict soil evidence for profound quaternary aridification of the Atacama Desert, Chile. Geoderma 267, 196–206.

Eghbal, M.K., Hamzehpour, N., Farpoor, M.H., 2018. Geology and geomorphology, in: The Soils of Iran. Springer, pp. 35–56.

Eswaran, H., Van den Berg, E., Reich, P., Kimble, J., 1995. Global soil carbon resources. Soils Glob. Chang. 27–43.

Ewing, S.A., Macalady, J.L., Warren-Rhodes, K., McKay, C.P., Amundson, R., 2008. Changes in the soil C cycle at the arid-hyperarid transition in the Atacama Desert. J. Geophys. Res. Biogeosciences 113.

Ewing, S.A., Sutter, B., Owen, J., Nishiizumi, K., Sharp, W., Cliff, S.S., Perry, K., Dietrich, W., McKay, C.P., Amundson, R., 2006. A threshold in soil formation at Earth's arid–hyperarid transition. Geochim. Cosmochim. Acta 70, 5293–5322.

Eze, S., Palmer, S.M., Chapman, P.J., 2018. Soil organic carbon stock in grasslands: Effects of inorganic fertilizers, liming and grazing in different climate settings. J. Environ. Manage. 223, 74–84.

Fa, K., Liu, Z., Zhang, Y., Qin, S., Wu, B., Liu, J., 2016. Abiotic carbonate dissolution traps carbon in a semiarid desert. Sci. Rep. 6.

Falsone, G., Catoni, M., Bonifacio, E., 2010. Effects of calcite on the soil porous structure: natural and experimental conditions. Agrochimica 54, 1–12.

Fathololoumi, S., Vaezi, A.R., Alavipanah, S.K., Ghorbani, A., Saurette, D., Biswas, A., 2020.

Improved digital soil mapping with multitemporal remotely sensed satellite data fusion: A case study in Iran. Sci. Total Environ. 721, 137703.

Ferdush, J., Paul, V., 2021. A review on the possible factors influencing soil inorganic carbon under elevated CO2. CATENA 204, 105434.

Fernández-Ugalde, O., Virto, I., Barré, P., Gartzia-Bengoetxea, N., Enrique, A., Imaz, M.J., Bescansa, P., 2011. Effect of carbonates on the hierarchical model of aggregation in calcareous semi-arid Mediterranean soils. Geoderma 164, 203–214.

Fey, M., 2010. Soils of South Africa. Cambridge University Press.

Filipová, L., Hédl, R., Covacevich, N., 2010. Variability of soil types in wetland meadows in the south of the Chilean Patagonia.

Filippi, P., Cattle, S.R., Pringle, M.J., Bishop, T.F.A., 2020. A two-step modelling approach to map the occurrence and quantity of soil inorganic carbon. Geoderma 371, 114382.

Finstad, K., Pfeiffer, M., Amundson, R., 2014. Hyperarid soils and the soil taxonomy. Soil Sci. Soc. Am. J. 78, 1845–1851.

Finstad, K., Pfeiffer, M., McNicol, G., Barnes, J., Demergasso, C., Chong, G., Amundson, R., 2016. Rates and geochemical processes of soil and salt crust formation in Salars of the Atacama Desert, Chile. Geoderma 284, 57–72.

Fornara, D.A., Steinbeiss, S., McNamara, N.P., Gleixner, G., Oakley, S., Poulton, P.R., Macdonald, A.J., Bardgett, R.D., 2011. Increases in soil organic carbon sequestration can reduce the global warming potential of long-term liming to permanent grassland. Glob. Chang. Biol. 17, 1925–1934.

Gaffey, S.J., 1986. Spectral reflectance of carbonate minerals in the visible and near infrared (0.35-2.55 microns); calcite, aragonite, and dolomite. Am. Mineral. 71, 151–162.

Garreaud, R., Vuille, M., Compagnucci, R., Marengo, J., n.d. Present-day South American climate, Paleogeogr. Palaeoclim. Paleoecol.

Gaspar, L., Mabit, L., Lizaga, I., Navas, A., 2020. Lateral mobilization of soil carbon induced by runoff along karstic slopes. J. Environ. Manage. 260, 110091.

Gaspar, L., Quijano, L., Lizaga, I., Navas, A., 2019. Effects of land use on soil organic and

inorganic C and N at 137Cs traced erosional and depositional sites in mountain agroecosystems. Catena 181, 104058.

Gaur, M.K., Squires, V.R., 2018. Geographic extent and characteristics of the world's arid zones and their peoples, in: Climate Variability Impacts on Land Use and Livelihoods in Drylands. Springer, pp. 3–20.

Gile, L.H., 1977. Holocene soils and soil-geomorphic relations in a semiarid region of southern New Mexico. Quat. Res. 7, 112–132.

Gile, L.H., Peterson, F.F., Grossman, R.B., 1966. Morphological and genetic sequences of carbonate accumulation in desert soils. Soil Sci. 101, 347–360.

Gocke, M., Pustovoytov, K., Kuzyakov, Y., 2011. Carbonate recrystallization in root-free soil and rhizosphere of Triticum aestivum and Lolium perenne estimated by 14C labeling. Biogeochemistry 103, 209–222.

Gomez, C., Adeline, K., Bacha, S., Driessen, B., Gorretta, N., Lagacherie, P., Roger, J.-M., Briottet, X., 2018. Sensitivity of clay content prediction to spectral configuration of VNIR/SWIR imaging data, from multispectral to hyperspectral scenarios. Remote Sens. Environ. 204, 18–30.

Gomez, C., Chevallier, T., Moulin, P., Arrouays, D., Barthès, B.G., 2022. Using carbonate absorbance peak to select the most suitable regression model before predicting soil inorganic carbon concentration by mid-infrared reflectance spectroscopy. Geoderma 405, 115403.

Gomez, C., Lagacherie, P., Coulouma, G., 2012. Regional predictions of eight common soil properties and their spatial structures from hyperspectral Vis–NIR data. Geoderma 189, 176–185.

Gomez, C., Lagacherie, P., Coulouma, G., 2008a. Continuum removal versus PLSR method for clay and calcium carbonate content estimation from laboratory and airborne hyperspectral measurements. Geoderma 148, 141–148.

Gomez, C., Rossel, R.A.V., McBratney, A.B., 2008b. Soil organic carbon prediction by hyperspectral remote sensing and field vis-NIR spectroscopy: An Australian case study. Geoderma 146, 403–411.

Grinand, C., Barthès, B.G., Brunet, D., Kouakoua, E., Arrouays, D., Jolivet, C., Caria, G., Bernoux, M., 2012. Prediction of soil organic and inorganic carbon contents at a national scale (France) using mid-infrared reflectance spectroscopy (MIRS). Eur. J. Soil Sci. 63, 141–151.

Groshans, G.R., Mikhailova, E.A., Post, C.J., Schlautman, M.A., Zhang, L., 2019. Determining the value of soil inorganic carbon stocks in the contiguous United States based on the avoided social cost of carbon emissions. Resources 8, 119.

Group, S.C.W., 2018. Soil classification: a natural and anthropogenic system for South Africa. Pretoria Soil Irrig. Res. Institute, Dep. Agric. Dev. South Africa, Pretoria.

Gruszczyński, S., Gruszczyński, W., 2022. Supporting soil and land assessment with machine learning models using the Vis-NIR spectral response. Geoderma 405, 115451.

Guglielmo, M., Zambonini, D., Porta, G., Malik, A., Tang, F.H.M., Maggi, F., 2021. Time-and depth-resolved mechanistic assessment of water stress in Australian ecosystems under the CMIP6 scenarios. Adv. Water Resour. 148, 103837.

Guo, Y., Amundson, R., Gong, P., Yu, Q., 2006a. Quantity and spatial variability of soil carbon in the conterminous United States. Soil Sci. Soc. Am. J. 70, 590–600.

Guo, Y., Gong, P., Amundson, R., Yu, Q., 2006b. Analysis of factors controlling soil carbon in the conterminous United States. Soil Sci. Soc. Am. J. 70, 601–612.

Guo, Y., Wang, X., Li, X., Wang, J., Xu, M., Li, D., 2016. Dynamics of soil organic and inorganic carbon in the cropland of upper Yellow River Delta, China. Sci. Rep. 6, 1–10.

Hamdi, S., Moyano, F., Sall, S., Bernoux, M., Chevallier, T., 2013. Synthesis analysis of the temperature sensitivity of soil respiration from laboratory studies in relation to incubation methods and soil conditions. Soil Biol. Biochem. 58, 115–126.

Hamilton, S.K., Kurzman, A.L., Arango, C., Jin, L., Robertson, G.P., 2007. Evidence for carbon sequestration by agricultural liming. Global Biogeochem. Cycles 21.

Haque, F., Santos, R.M., Chiang, Y.W., 2020. CO2 sequestration by wollastonite-amended agricultural soils–An Ontario field study. Int. J. Greenh. Gas Control 97, 103017.

Hartmann, J., 2009. Bicarbonate-fluxes and CO2-consumption by chemical weathering on the

Japanese Archipelago—application of a multi-lithological model framework. Chem. Geol. 265, 237–271.

Hasinger, O., Spangenberg, J.E., Millière, L., Bindschedler, S., Cailleau, G., Verrecchia, E.P., 2015. Carbon dioxide in scree slope deposits: A pathway from atmosphere to pedogenic carbonate. Geoderma 247, 129–139.

Havlin, J.L., 2014. Soil fertility and nutrient management. Up. Saddle River, NJ, USA 460–469.

Isbell, R., 2016. The Australian soil classification. CSIRO publishing.

Jenny, H., Leonard, C.D., 1934. Functional relationships between soil properties and rainfall. Soil Sci. 38, 363–382.

Jiménez-Aguirre, M.T., Isidoro, D., Usón, A., 2018. Soil variability in la Violada Irrigation District (Spain): I delineating soil units for irrigation. Geoderma 311, 78–90.

Joel, A.H., Smoot, C.C., Cooperrider, C.K., Slater, C.S., Bratley, C.O., Cuvillier, E., Hepting, G.H., Schnur, G.L., Barber, G.W., Musgrave, G.W., 1937. Soil erosion and stream flow on range and forest lands of the upper Rio Grande watershed in relation to land resources and human welfare. US Department of Agriculture.

Jones, A., Montanarella, L., Jones, R., 2005. Soil atlas of Europe. European Commission.

Jordaan, G.J., Kilian, A., Muthivelli, N., Dlamini, D., 2017. Practical Application of Nano-technology in Roads in southern Africa, in: Proceedings of the 8th Transportation Technology Transfer (T2) Conference, Lusaka, Zambia. pp. 8–10.

Kasraei, B., Heung, B., Saurette, D.D., Schmidt, M.G., Bulmer, C.E., Bethel, W., 2021. Quantile regression as a generic approach for estimating uncertainty of digital soil maps produced from machine-learning. Environ. Model. Softw. 144, 105139.

Keskin, H., Grunwald, S., Harris, W.G., 2019. Digital mapping of soil carbon fractions with machine learning. Geoderma 339, 40–58.

Khormali, F., Toomanian, N., 2018. Soil-forming factors and processes, in: The Soils of Iran. Springer, pp. 73–91.

Kim, J.H., Jobbágy, E.G., Richter, D.D., Trumbore, S.E., Jackson, R.B., 2020. Agricultural acceleration of soil carbonate weathering. Glob. Chang. Biol. 26, 5988–6002.

Kuzyakov, Y., Horwath, W.R., Dorodnikov, M., Blagodatskaya, E., 2019. Review and synthesis of the effects of elevated atmospheric CO2 on soil processes: No changes in pools, but increased fluxes and accelerated cycles. Soil Biol. Biochem. 128, 66–78.

Lagacherie, P., Alvaro-Fuentes, J., Annabi, M., Bernoux, M., Bouarfa, S., Douaoui, A., Grünberger, O., Hammani, A., Montanarella, L., Mrabet, R., 2018. Managing Mediterranean soil resources under global change: expected trends and mitigation strategies. Reg. Environ. Chang. 18, 663–675.

Lagacherie, P., Baret, F., Feret, J.-B., Netto, J.M., Robbez-Masson, J.M., 2008. Estimation of soil clay and calcium carbonate using laboratory, field and airborne hyperspectral measurements. Remote Sens. Environ. 112, 825–835.

Lal, R., Kimble, J.M., Stewart, B.A., Eswaran, H., 1999. Global climate change and pedogenic carbonates.

Lamichhane, S., Kumar, L., Wilson, B., 2019. Digital soil mapping algorithms and covariates for soil organic carbon mapping and their implications: A review. Geoderma 352, 395–413.

Landeweert, R., Hoffland, E., Finlay, R.D., Kuyper, T.W., van Breemen, N., 2001. Linking plants to rocks: ectomycorrhizal fungi mobilize nutrients from minerals. Trends Ecol. Evol. 16, 248–254.

Landi, A., Mermut, A.R., Anderson, D.W., 2003. Origin and rate of pedogenic carbonate accumulation in Saskatchewan soils, Canada. Geoderma 117, 143–156.

Lapenis, A.G., Lawrence, G.B., Bailey, S.W., Aparin, B.F., Shiklomanov, A.I., Speranskaya, N.A., Torn, M.S., Calef, M., 2008. Climatically driven loss of calcium in steppe soil as a sink for atmospheric carbon. Global Biogeochem. Cycles 22.

Laudicina, V.A., Dazzi, C., Delgado, A., Barros, H., Scalenghe, R., 2021. Relief and calcium from gypsum as key factors for net inorganic carbon accumulation in soils of a semiarid Mediterranean environment. Geoderma 398, 115115.

Laudicina, V.A., Scalenghe, R., Pisciotta, A., Parello, F., Dazzi, C., 2013. Pedogenic carbonates and carbon pools in gypsiferous soils of a semiarid Mediterranean environment in south Italy. Geoderma 192, 31–38.

Legodi, M.A., De Waal, D., Potgieter, J.H., Potgieter, S.S., 2001. Rapid determination of CaCO3 in mixtures utilising FT—IR spectroscopy. Miner. Eng. 14, 1107–1111.

Leogrande, R., Vitti, C., Castellini, M., Mastrangelo, M., Pedrero, F., Vivaldi, G.A., Stellacci, A.M., 2021. Comparison of Two Methods for Total Inorganic Carbon Estimation in Three Soil Types in Mediterranean Area. Land 10, 409.

Lettens, S., Van Orshoven, J., van Wesemael, B., Muys, B., 2004. Soil organic and inorganic carbon contents of landscape units in Belgium derived using data from 1950 to 1970. Soil Use Manag. 20, 40–47.

Li, J., Awasthi, M.K., Zhu, Q., Chen, X., Wu, Faqi, Wu, Fuyong, Tong, X., 2021. Modified soil physicochemical properties promoted sequestration of organic and inorganic carbon synergistically during revegetation in desertified land. J. Environ. Chem. Eng. 106331.

Liu, W., Wei, J., Cheng, J., Li, W., 2014. Profile distribution of soil inorganic carbon along a chronosequence of grassland restoration on a 22-year scale in the Chinese Loess Plateau. Catena 121, 321–329.

Loeppert, R.H., Suarez, D.L., 1996. Carbonate and gypsum.

Loke, P.F., Kotzé, E., Du Preez, C.C., Twigge, L., 2021. Cross-rangeland comparisons on soil carbon dynamics in the pedoderm of semi-arid and arid South African commercial farms. Geoderma 381, 114689.

Lovegrove, B.G., Siegfried, W.R., 1986. Distribution and formation of Mima-like earth mounds in the western Cape Province of South Africa. S. Afr. J. Sci. 82, 432–436.

Lozbenev, N., Yurova, A., Smirnova, M., Kozlov, D., 2021. Incorporating process-based modeling into digital soil mapping: A case study in the virgin steppe of the Central Russian Upland. Geoderma 383, 114733.

Lu, T., Wang, X., Zhang, W., 2020. Total and dissolved soil organic and inorganic carbon and their relationships in typical loess cropland of Fengu Basin. Geosci. Lett. 7, 1–13.

Mahmoudabadi, E., Karimi, A., Haghnia, G.H., Sepehr, A., 2017. Digital soil mapping using remote sensing indices, terrain attributes, and vegetation features in the rangelands of northeastern Iran. Environ. Monit. Assess. 189, 1–20.

Mammadov, E., Nowosad, J., Glaesser, C., 2021. Estimation and mapping of surface soil properties in the Caucasus Mountains, Azerbaijan using high-resolution remote sensing data. Geoderma Reg. e00411.

Marbut, C.F., 1935. Soils of the United States, atlas of American agriculture, Part III. US Dep. Agric. Washington, DC.

Marchant, B.P., Villanneau, E.J., Arrouays, D., Saby, N.P.A., Rawlins, B.G., 2015. Quantifying and mapping topsoil inorganic carbon concentrations and stocks: approaches tested in France. Soil Use Manag. 31, 29–38.

Martí-Roura, M., Hagedorn, F., Rovira, P., Romanyà, J., 2019. Effect of land use and carbonates on organic matter stabilization and microbial communities in Mediterranean soils. Geoderma 351, 103–115.

Martin, J.B., 2017. Carbonate minerals in the global carbon cycle. Chem. Geol. 449, 58–72.

Martin, M.P., Dimassi, B., Román Dobarco, M., Guenet, B., Arrouays, D., Angers, D.A., Blache, F., Huard, F., Soussana, J., Pellerin, S., 2021. Feasibility of the 4 per 1000 aspirational target for soil carbon: A case study for France. Glob. Chang. Biol. 27, 2458–2477.

McBratney, A.B., Santos, M.L.M., Minasny, B., 2003. On digital soil mapping. Geoderma 117, 3–52.

Mi, N.A., Wang, S., Liu, J., Yu, G., Zhang, W., Jobbagy, E., 2008. Soil inorganic carbon storage pattern in China. Glob. Chang. Biol. 14, 2380–2387.

Mikhailova, E.A., Post, C.J., 2006. Effects of land use on soil inorganic carbon stocks in the Russian Chernozem. J. Environ. Qual. 35, 1384–1388.

Miklos, M., Short, M.G., McBratney, A.B., Minasny, B., 2010. Mapping and comparing the distribution of soil carbon under cropping and grazing management practices in Narrabri, north-west New South Wales. Soil Res. 48, 248–257.

Minasny, B., McBratney, A.B., 2016. Digital soil mapping: A brief history and some lessons. Geoderma 264, 301–311.

Mirzaeitalarposhti, R., Demyan, M.S., Rasche, F., Cadisch, G., Müller, T., 2017. Mid-infrared spectroscopy to support regional-scale digital soil mapping on selected croplands of South-

West Germany. Catena 149, 283–293.

Mitran, T., Sreenivas, K., Janakirama Suresh, K.G., Sujatha, G., Ravisankar, T., 2021. Spatial Prediction of Calcium Carbonate and Clay Content in Soils using Airborne Hyperspectral Data. J. Indian Soc. Remote Sens. 1–12.

Mohseni, N., Salar, Y.S., 2021. Terrain indices control the quality of soil total carbon stock within water erosion-prone environments. Ecohydrol. Hydrobiol. 21, 46–54.

Monger, H.C., Bestelmeyer, B.T., 2006. The soil-geomorphic template and biotic change in arid and semi-arid ecosystems. J. Arid Environ. 65, 207–218.

Monger, H.C., Kraimer, R.A., Khresat, S., Cole, D.R., Wang, X., Wang, J., 2015. Sequestration of inorganic carbon in soil and groundwater. Geology 43, 375–378.

Mosleh, Z., Salehi, M.H., Jafari, A., Borujeni, I.E., Mehnatkesh, A., 2016. The effectiveness of digital soil mapping to predict soil properties over low-relief areas. Environ. Monit. Assess. 188, 195.

Mulder, V.L., de Bruin, S., Weyermann, J., Kokaly, R.F., Schaepman, M.E., 2013. Characterizing regional soil mineral composition using spectroscopy and geostatistics. Remote Sens. Environ. 139, 415–429.

Nayak, A.K., Rahman, M.M., Naidu, R., Dhal, B., Swain, C.K., Nayak, A.D., Tripathi, R., Shahid, M., Islam, M.R., Pathak, H., 2019. Current and emerging methodologies for estimating carbon sequestration in agricultural soils: A review. Sci. Total Environ. 665, 890–912.

Nelson, D.W., Sommers, L.E., 1996. Total carbon, organic carbon, and organic matter. Methods soil Anal. Part 3 Chem. methods 5, 961–1010.

Nguyen, T.T., Janik, L.J., Raupach, M., 1991. Diffuse reflectance infrared Fourier transform (DRIFT) spectroscopy in soil studies. Soil Res. 29, 49–67.

NRCS, U., 2006. Land resource regions and major land resource areas of the United States, the Caribbean, and the Pacific Basin. USDA Handbook 296. US Dep. Agric. Nat. Resour. Conserv. Serv. Washington, DC, USA.

Okyay, T.O., Rodrigues, D.F., 2015. Biotic and abiotic effects on CO_2 sequestration during

microbially-induced calcium carbonate precipitation. FEMS Microbiol. Ecol. 91.

ORGANIZATION-FAO, F.A.N.D.A., [FAO]., F. and A.O., 2014. World reference base for soil resources 2014: International soil classification system for naming soils and creating legends for soil maps. World Soil Resour. Rep. No 106.

Owen, J.J., Amundson, R., Dietrich, W.E., Nishiizumi, K., Sutter, B., Chong, G., 2011. The sensitivity of hillslope bedrock erosion to precipitation. Earth Surf. Process. Landforms 36, 117–135.

Padarian, J., Minasny, B., McBratney, A.B., Smith, P., 2021. Additional soil organic carbon storage potential in global croplands. SOIL Discuss. 1–15.

Padarian, J., Pfeiffer, M., Vega, M. P., Estay, K. 2022 Distribution of pedogenic calcium carbonates along Chile's climatic gradient. (Under review).

Paradelo, R., Virto, I., Chenu, C., 2015. Net effect of liming on soil organic carbon stocks: a review. Agric. Ecosyst. Environ. 202, 98–107.

Paterson, G., Turner, D., Wiese, L., Van Zijl, G., Clarke, C., Van Tol, J., 2015. Spatial soil information in South Africa: Situational analysis, limitations and challenges. S. Afr. J. Sci. 111, 1–7.

Pfeiffer, M., Aburto, F., Le Roux, J.P., Kemnitz, H., Sedov, S., Solleiro-Rebolledo, E., Seguel, O., 2012. Development of a Pleistocene calcrete over a sequence of marine terraces at Tongoy (north-central Chile) and its paleoenvironmental implications. Catena 97, 104–118.

Pfeiffer, M., Latorre, C., Gayo, E., Amundson, R., 2019. Rare calcium chloride–rich soil and implications for the existence of liquid water in a hyperarid environment. Geology 47, 163–166.

Pfeiffer, M., Latorre, C., Santoro, C.M., Gayo, E.M., Rojas, R., Carrevedo, M.L., McRostie, V.B., Finstad, K.M., Heimsath, A., Jungers, M.C., 2018. Chronology, stratigraphy and hydrological modelling of extensive wetlands and paleolakes in the hyperarid core of the Atacama Desert during the late quaternary. Quat. Sci. Rev. 197, 224–245.

Pfeiffer, M., Le Roux, J.P., Solleiro-Rebolledo, E., Kemnitz, H., Sedov, S., Seguel, O., 2011. Preservation of beach ridges due to pedogenic calcrete development in the Tongoy

palaeobay, North-Central Chile. Geomorphology 132, 234–248.

Pfeiffer, M., Morgan, A., Heimsath, A., Jordan, T., Howard, A., Amundson, R., 2021. Century scale rainfall in the absolute Atacama Desert: landscape response and implications for past and future rainfall. Quat. Sci. Rev. 254, 106797.

Piccini, C., Marchetti, A., Rivieccio, R., Napoli, R., 2019. Multinomial logistic regression with soil diagnostic features and land surface parameters for soil mapping of Latium (Central Italy). Geoderma 352, 385–394.

Picker, M.D., Hoffman, M.T., Leverton, B., 2007. Density of Microhodotermes viator (Hodotermitidae) mounds in southern Africa in relation to rainfall and vegetative productivity gradients. J. Zool. 271, 37–44.

Poppiel, R.R., Demattê, J.A.M., Rosin, N.A., Campos, L.R., Tayebi, M., Bonfatti, B.R., Ayoubi, S., Tajik, S., Afshar, F.A., Jafari, A., 2021. High resolution middle eastern soil attributes mapping via open data and cloud computing. Geoderma 385, 114890.

Quade, J., Rech, J.A., Latorre, C., Betancourt, J.L., Gleeson, E., Kalin, M.T.K., 2007. Soils at the hyperarid margin: the isotopic composition of soil carbonate from the Atacama Desert, Northern Chile. Geochim. Cosmochim. Acta 71, 3772–3795.

Raheb, A., Heidari, A., Mahmoodi, S., 2017. Organic and inorganic carbon storage in soils along an arid to dry sub-humid climosequence in northwest of Iran. CATENA 153, 66–74.

Ramnarine, R., Wagner-Riddle, C., Dunfield, K.E., Voroney, R.P., 2012. Contributions of carbonates to soil CO_2 emissions. Can. J. Soil Sci. 92, 599–607.

Rasmussen, C., 2006. Distribution of soil organic and inorganic carbon pools by biome and soil taxa in Arizona. Soil Sci. Soc. Am. J. 70, 256–265.

Raza, S., Zamanian, K., Ullah, S., Kuzyakov, Y., Virto, I., Zhou, J., 2021. Inorganic carbon losses by soil acidification jeopardize global efforts on carbon sequestration and climate change mitigation. J. Clean. Prod. 128036.

Rech, J.A., Quade, J., Hart, W.S., 2003. Isotopic evidence for the source of Ca and S in soil gypsum, anhydrite and calcite in the Atacama Desert, Chile. Geochim. Cosmochim. Acta 67, 575–586.

Retallack, G.J., 1994. The environmental factor approach to the interpretation of paleosols. Factors soil Form. A fiftieth Anniv. Retrosp. 33, 31–64.

Roozitalab, M.H., Siadat, H., Farshad, A., 2018a. The soils of Iran. Springer.

Roozitalab, M.H., Toomanian, N., Dehkordi, V.R.G., Khormali, F., 2018b. Major soils, properties, and classification, in: The Soils of Iran. Springer, pp. 93–147.

Rossel, R.A.V., Walvoort, D.J.J., McBratney, A.B., Janik, L.J., Skjemstad, J.O., 2006. Visible, near infrared, mid infrared or combined diffuse reflectance spectroscopy for simultaneous assessment of various soil properties. Geoderma 131, 59–75.

Rowley, M.C., Grand, S., Verrecchia, É.P., 2018. Calcium-mediated stabilisation of soil organic carbon. Biogeochemistry 137, 27–49.

Royer, D.L., 1999. Depth to pedogenic carbonate horizon as a paleoprecipitation indicator? Geology 27, 1123–1126.

Saby, N.P.A., Swiderski, C., Lemercier, B., Walter, C., Louis, B.P., Eveillard, P., Arrouays, D., 2017. Is pH increasing in the noncalcareous topsoils of France under agricultural management? A statistical framework to overcome the limitations of a soil test database. Soil Use Manag. 33, 460–470.

Salley, S.W., Sleezer, R.O., Bergstrom, R.M., Martin, P.H., Kelly, E.F., 2016. A long-term analysis of the historical dry boundary for the Great Plains of North America: Implications of climatic variability and climatic change on temporal and spatial patterns in soil moisture. Geoderma 274, 104–113.

Schlesinger, W.H., 1985. The formation of caliche in soils of the Mojave Desert, California. Geochim. Cosmochim. Acta 49, 57–66.

Schlesinger, W.H., Reynolds, J.F., Cunningham, G.L., Huenneke, L.F., Jarrell, W.M., Virginia, R.A., Whitford, W.G., 1990. Biological feedbacks in global desertification. Science (80-.). 247, 1043–1048.

Sepahvand, H., Mirzaeitalarposhti, R., Beiranvand, K., Feizian, M., Müeller, T., 2019. Prediction of soil carbon levels in calcareous soils of Iran by mid-infrared reflectance spectroscopy. Environ. Pollut. Bioavailab. 31, 9–17.

Serna-Pérez, A., Monger, H.C., Herrick, J.E., Murray, L., 2006. Carbon dioxide emissions from exhumed petrocalcic horizons. Soil Sci. Soc. Am. J. 70, 795–805.

Seybold, C.A., Ferguson, R., Wysocki, D., Bailey, S., Anderson, J., Nester, B., Schoeneberger, P., Wills, S., Libohova, Z., Hoover, D., 2019. Application of mid-infrared spectroscopy in soil survey. Soil Sci. Soc. Am. J. 83, 1746–1759.

Sharififar, A., Sarmadian, F., Alikhani, H., Keshavarzi, A., Asghari, O., Malone, B.P., 2019. Lateral and Vertical Variations of Soil Organic and Inorganic Carbon Content in Aridisols and Entisols of a Rangeland. Eurasian Soil Sci. 52. https://doi.org/10.1134/S1064229319090084

Sharififar, Amin, Sarmadian, F., Minasny, B., 2019. Mapping imbalanced soil classes using Markov chain random fields models treated with data resampling technique. Comput. Electron. Agric. 159, 110–118.

Sherrod, L.A., Erskine, R.H., Green, T.R., 2015. Spatial Patterns and Cross-Correlations of Temporal Changes in Soil Carbonates and Surface Elevation in a Winter Wheat–Fallow Cropping System. Soil Sci. Soc. Am. J. 79, 417–427.

Shi, Y., Baumann, F., Ma, Y., Song, C., Kühn, P., Scholten, T., He, J.-S., 2012. Organic and inorganic carbon in the topsoil of the Mongolian and Tibetan grasslands: pattern, control and implications. Biogeosciences 9, 2287–2299.

Song, X.-D., Yang, F., Wu, H.-Y., Zhang, J., Li, D.-C., Liu, F., Zhao, Y.-G., Yang, J.-L., Ju, B., Cai, C.-F., 2022. Significant loss of soil inorganic carbon at the continental scale. Natl. Sci. Rev. 9, nwab120.

Sreenivas, K., Dadhwal, V.K., Kumar, S., Harsha, G.S., Mitran, T., Sujatha, G., Suresh, G.J.R., Fyzee, M.A., Ravisankar, T., 2016. Digital mapping of soil organic and inorganic carbon status in India. Geoderma 269, 160–173.

Staff, L.T.S., 1972. Land types of South Africa: Digital map (1: 250 000 scale) and soil inventory databases.

Stevenson, B.A., Kelly, E.F., McDonald, E.V., Busacca, A.J., 2005. The stable carbon isotope composition of soil organic carbon and pedogenic carbonates along a bioclimatic gradient in the Palouse region, Washington State, USA. Geoderma 124, 37–47.

Tan, W.-F., Zhang, R., Cao, H., Huang, C.-Q., Yang, Q.-K., Wang, M., Koopal, L.K., 2014. Soil inorganic carbon stock under different soil types and land uses on the Loess Plateau region of China. Catena 121, 22–30.

Tao, J., Raza, S., Zhao, M., Cui, J., Wang, P., Sui, Y., Zamanian, K., Kuzyakov, Y., Xu, M., Chen, Z., 2022. Vulnerability and driving factors of soil inorganic carbon stocks in Chinese croplands. Sci. Total Environ. 825, 154087.

Targulian, V.O., Goryachkin, S. V, 2004. Soil memory: Types of record, carriers, hierarchy and diversity. Rev. Mex. Ciencias Geológicas 21, 1–8.

Tong, L.S., Fang, N.F., Xiao, H.B., Shi, Z.H., 2020. Sediment deposition changes the relationship between soil organic and inorganic carbon: Evidence from the Chinese Loess Plateau. Agric. Ecosyst. Environ. 302, 107076.

Vaudour, E., Gomez, C., Fouad, Y., Lagacherie, P., 2019. Sentinel-2 image capacities to predict common topsoil properties of temperate and Mediterranean agroecosystems. Remote Sens. Environ. 223, 21–33.

Vera, W., 1985. Mineralogy and micromorphology of calcium carbonate-rich soils from Chile.

Vial, C.D., 1965. Soils of the arid zones of Chile. FAO.

Wang, J., Wang, X., Zhang, J., 2018. Land Use Impacts on Soil Organic and Inorganic Carbon and Their Isotopes in the Yanqi Basin, in: Carbon Cycle in the Changing Arid Land of China. Springer, pp. 69–88.

Wang, L., Huang, X., Fang, N.F., Niu, Y.H., Wang, T.W., Shi, Z.H., 2019. Selective transport of soil organic and inorganic carbon in eroded sediment in response to raindrop sizes and inflow rates in rainstorms. J. Hydrol. 575, 42–53.

Wang, X., Wang, J., Xu, M., Zhang, W., Fan, T., Zhang, J., 2015. Carbon accumulation in arid croplands of northwest China: pedogenic carbonate exceeding organic carbon. Sci. Rep. 5, 1–12.

Wang, X., Wang, J., Zhang, J., 2012. Comparisons of three methods for organic and inorganic carbon in calcareous soils of northwestern China.

Wang, X.J., Xu, M.G., Wang, J.P., Zhang, W.J., Yang, X.Y., Huang, S.M., Liu, H., 2014.

Fertilization enhancing carbon sequestration as carbonate in arid cropland: assessments of long-term experiments in northern China. Plant Soil 380, 89–100.

Wang, Y., Li, Y., Ye, X., Chu, Y., Wang, X., 2010. Profile storage of organic/inorganic carbon in soil: From forest to desert. Sci. Total Environ. 408, 1925–1931.

Weinert, H.H., 1980. Natural road construction materials of Southern Africa. CSIR.

White, R.P., Nackoney, J., 2003. Drylands, people, and ecosystem goods and services: a web-based geospatial analysis (PDF version). World Resour. Inst. ([Available http//pdf. wri. org/drylands. pdf accessed 30/01/2012]).

Wijewardane, N.K., Ge, Y., Wills, S., Libohova, Z., 2018. Predicting physical and chemical properties of US soils with a mid-infrared reflectance spectral library. Soil Sci. Soc. Am. J. 82, 722–731.

Wilford, J., De Caritat, P., Bui, E., 2015. Modelling the abundance of soil calcium carbonate across Australia using geochemical survey data and environmental predictors. Geoderma 259, 81–92.

Williams, C.J.R., 2017. Climate change in Chile: An analysis of state-of-the-art observations, satellite-derived estimates and climate model simulations. J. Earth Sci. Clim. Chang 8, 400.

WILLIAMS, P.C., 1987. Qualitative applications of near infrared reflectance spectroscopy. Near-infrared Technol. Agric. Food Ind.

Wu, H., Guo, Z., Gao, Q., Peng, C., 2009. Distribution of soil inorganic carbon storage and its changes due to agricultural land use activity in China. Agric. Ecosyst. Environ. 129, 413–421.

Xia, J., Ning, L., Wang, Q., Chen, J., Wan, L., Hong, S., 2017. Vulnerability of and risk to water resources in arid and semi-arid regions of West China under a scenario of climate change. Clim. Change 144, 549–563.

Xiao, D., Huang, Y., Feng, S., Ge, Y., Zhang, W., He, X., Wang, K., 2018. Soil organic carbon mineralization with fresh organic substrate and inorganic carbon additions in a red soil is controlled by fungal diversity along a pH gradient. Geoderma 321, 79–89.

Xie, Y., Huang, F., Yang, H., Yu, S., 2021. Role of anthropogenic sulfuric and nitric acids in

carbonate weathering and associated carbon sink budget in a karst catchment (Guohua), southwestern China. J. Hydrol. 599, 126287.

Yaalon, D.H., 1987. Saharan dust and desert loess: effect on surrounding soils. J. African Earth Sci. 6, 569–571.

Yang, G.U.O., Xiujun, W., Xianglan, L.I., Minggang, X.U., Yuan, L.I., Zheng, H., Yongming, L.U.O., Smith, P., 2021. Impacts of land use and salinization on soil inorganic and organic carbon in the middle-lower Yellow River Delta. Pedosphere 31, 839–848.

Yang, P., Shu, Q., Liu, Q., Hu, Z., Zhang, S., Ma, Y., 2021. Distribution and factors influencing organic and inorganic carbon in surface sediments of tidal flats in northern Jiangsu, China. Ecol. Indic. 126, 107633.

Yang, R.-M., Yang, Fan, Yang, Fei, Huang, L.-M., Liu, F., Yang, J.-L., Zhao, Y.-G., Li, D.-C., Zhang, G.-L., 2017. Pedogenic knowledge-aided modelling of soil inorganic carbon stocks in an alpine environment. Sci. Total Environ. 599, 1445–1453.

You, M., Han, X., Hu, N., Du, S., Doane, T.A., Li, L.-J., 2020. Profile storage and vertical distribution (0–150 cm) of soil inorganic carbon in croplands in northeast China. Catena 185, 104302.

Zamanian, K., Kuzyakov, Y., 2019. Contribution of soil inorganic carbon to atmospheric CO2: More important than previously thought. Glob. Chang. Biol 25, E1–E3.

Zamanian, K., Pustovoytov, K., Kuzyakov, Y., 2016. Pedogenic carbonates: Forms and formation processes. Earth-Science Rev. 157, 1–17.

Zamanian, K., Zarebanadkouki, M., Kuzyakov, Y., 2018. Nitrogen fertilization raises CO2 efflux from inorganic carbon: A global assessment. Glob. Chang. Biol. 24, 2810–2817.

Zamanian, K., Zhou, J., Kuzyakov, Y., 2021. Soil carbonates: The unaccounted, irrecoverable carbon source. Geoderma 384, 114817.

Zeraatpisheh, M., Ayoubi, S., Jafari, A., Tajik, S., Finke, P., 2019. Digital mapping of soil properties using multiple machine learning in a semi-arid region, central Iran. Geoderma 338, 445–452.

Zhang, H., Yin, A., Yang, X., Wu, P., Fan, M., Wu, J., Zhang, M., Gao, C., 2019. Changes in

surface soil organic/inorganic carbon concentrations and their driving forces in reclaimed coastal tidal flats. Geoderma 352, 150–159.

Zhang, N., Xing-Dong, H.E., Yu-Bao, G.A.O., Yong-Hong, L.I., Hai-Tao, W., Di, M.A., Zhang, R., Yang, S., 2010. Pedogenic carbonate and soil dehydrogenase activity in response to soil organic matter in Artemisia ordosica community. Pedosphere 20, 229–235.

Zhao, W., Zhang, R., Cao, H., Tan, W., 2019. Factor contribution to soil organic and inorganic carbon accumulation in the Loess Plateau: structural equation modeling. Geoderma 352, 116–125.

Zissimos, A.M., Christoforou, I.C., Cohen, D.R., Mooney, S.D., Rutherford, N.F., 2019. Spatial distribution and controls on organic and inorganic carbon in the soils of Cyprus. J. Geochemical Explor. 196, 95–104.

Zornoza, R., Acosta, J.A., Gabarrón, M., Gómez-Garrido, M., Sánchez-Navarro, V., Terrero, A., Martínez-Martínez, S., Faz, Á., Pérez-Pastor, A., 2018. Greenhouse gas emissions and soil organic matter dynamics in woody crop orchards with different irrigation regimes. Sci. Total Environ. 644, 1429–1438.